Symmetric Subspace Motion Generators

This is the post peer-review accepted manuscript of:

Y. Wu and M. Carricato, "Symmetric Subspace Motion Generators"

in IEEE Transactions on Robotics, vol. 34, no. 3, pp. 716-735, June 2018.

doi: 10.1109/TRO.2018.2813377

The published version is available online at:
https://ieeexplore.ieee.org/stamp/stamp.jsp?tp=&arnumber=8355706

Symmetric Subspace Motion Generators

Yuanqing Wu, *Member, IEEE,* and Marco Carricato, *Member, IEEE*

***Abstract*—When moving an object endowed with continuous symmetry, an ambiguity arises in its underlying rigid body transformation, induced by the arbitrariness of the portion of motion that does not change the body overall shape. The functional redundancy caused by continuous symmetry is ubiquitously present in a broad range of robotic applications, including robot machining and haptic interface (revolute symmetry), remote center of motion devices for minimal invasive surgery (line symmetry), and motion modules for hyper-redundant robots (plane symmetry). In this paper, we argue that such functional redundancy can be systematically resolved by resorting to symmetric subspaces of the special Euclidean group $\mathrm{SE}(3)$, which motivates us to systematically investigate structural synthesis of symmetric subspace motion generators. In particular, we develop a general synthesis procedure that allows us to generate a wide spectrum of novel mechanisms for use in the aforesaid applications.**

***Index Terms*—Euclidean group, inversion symmetry, symmetric space, Lie triple system (LTS), type synthesis, parallel manipulator.**

NOMENCLATURE

$\mathrm{SE}(3)$	special Euclidean group of $\mathbb{R}^3$
$\mathrm{SO}(3)$	special orthogonal group of $\mathbb{R}^3$
$\mathrm{G}, \mathrm{H}, ...$	Lie subgroups of $\mathrm{SE}(3)$
$\mathfrak{se}(3)$	Lie algebra of $\mathrm{SE}(3)$
$[\cdot,\cdot]$	commutator (Lie bracket)
$\mathfrak{se}(3)^*$	dual space of $\mathfrak{se}(3)$ (wrench space)
$\mathfrak{so}(3)$	Lie algebra of $\mathrm{SO}(3)$
$\mathfrak{g}, \mathfrak{h}, ...$	Lie algebras of $\mathrm{G}, \mathrm{H}, ...$
$\{...\}_{\mathrm{span}}$	linear span
S, S_i	twist subspaces of $\mathfrak{se}(3)$
$S^\perp, S_i^\perp$	annihilator of S and S_i in $\mathfrak{se}(3)^*$
$\mathfrak{m}$	Lie triple subsystem (LTS) of $\mathfrak{se}(3)$
$\mathrm{M} := \exp \mathfrak{m}$	a symmetric subspace (SS) of $\mathrm{SE}(3)$
$\mathfrak{h}_\mathfrak{m} := [\mathfrak{m}, \mathfrak{m}]$	commutator algebra of $\mathfrak{m}$
$\mathfrak{g}_\mathfrak{m} := \mathfrak{m} + \mathfrak{h}_\mathfrak{m}$	completion algebra of $\mathfrak{m}$
$\mathrm{G}_\mathrm{M} := \exp \mathfrak{g}_\mathfrak{m}$	completion group of $\mathrm{M} = \exp \mathfrak{m}$
GPD	generalized polar decomposition
M, M_i	motion manifolds
POE	product-of-exponentials submanifold
$\mathcal{M}_i$	a serial chain with motion manifold M_i
PM	a (purely) parallel manipulator with l chains $\mathcal{M}_i, i = 1, ..., l$, denoted $\mathcal{M}_1 \| ... \| \mathcal{M}_l$
ICPM	an inter-connected parallel manipulator
SPHM	a serial-parallel hybrid manipulator
SP	symmetric twist pair
SC	symmetric twist chain
CSC	constraint synthesis condition Eq. (9b)
SMC	symmetric movement condition Eq. (16)
$\mathcal{M}_i^+$	proximal half of a SC $\mathcal{M}_i$
$\mathcal{M}_i^-$	distal half of a SC $\mathcal{M}_i$
$\mathcal{M}^+$	proximal PM of a SS-ICPM
$\mathcal{M}^-$	distal PM of a SS-ICPM

Yuanqing Wu (e-mail: yuanqing.wu@unibo.it) and Marco Carricato (e-mail: marco.carricato@unibo.it) are with Department of Industrial Engineering (DIN), University of Bologna, Italy.

I. INTRODUCTION

A. Motivation

ROBOTIC manipulation tasks requiring less-than-six degrees of freedom (DoF) can be naturally characterized by regular submanifolds of $\mathrm{SE}(3)$, which coincide with the end-effector motion set in an open neighborhood of the identity $\mathbf{I}$. We shall refer to them as *motion manifolds*. The most commonly used motion manifolds, aside from $\mathrm{SE}(3)$ itself, are its ten conjugacy classes of (connected) Lie subgroups [1]. For example, Franz Reuleaux's lower pairs (revolute $\mathcal{R}$, prismatic $\mathcal{P}$, helical $\mathcal{H}$, cylindrical $\mathcal{C}$, planar $\mathcal{E}$, spherical $\mathcal{S}$) generate 1 to 3D Lie subgroups of $\mathrm{SE}(3)$ [2]. Lie subgroups of $\mathrm{SE}(3)$ also serve as configuration spaces of a range of robotic systems [3]–[6].

Lie subgroups may also characterize the invariant motions of objects with continuous symmetry [7,8]. For example, when orientating the tool spindle of a five-axis milling task or rotating a round peg for a peg-in-hole assembly task, two rotations $\mathbf{R}_1, \mathbf{R}_2$ of the spindle or peg are said to be equivalent if they differ by an arbitrary rotation about their axis of revolute symmetry, say the $\mathbf{z}$-axis (see Fig. 1(a)):

$$\mathbf{R}_1 = \mathbf{R}_2 e^{\sigma \widehat{\mathbf{z}}} \quad \sigma \in \mathbb{R} \tag{1}$$

where $\mathbf{z}$ denotes the unit vector $(0,0,1)^T$, and $\widehat{\mathbf{z}}$ denotes the 3×3 skew-symmetric matrix satisfying $\widehat{\mathbf{z}}\mathbf{v} = \mathbf{z} \times \mathbf{v}, \forall \mathbf{v} \in \mathbb{R}^3$ (the notation used in this paper to denote the elements of $\mathrm{SE}(3)$ and its Lie algebra $\mathfrak{se}(3)$ is intended to be self-explanatory; however, a brief explanation is reported in Appendix A). To resolve such a functional redundancy [9], Bonev *et al.* [10] proposed a decomposition of $\mathrm{SO}(3)$ using the tilt-torsion angle parameterization of a rotation matrix $\mathbf{R} \in \mathrm{SO}(3)$ (see Fig. 1(b)):

$$\mathbf{R} = e^{\psi(c_\phi \widehat{\mathbf{x}} + s_\phi \widehat{\mathbf{y}})} e^{\sigma \widehat{\mathbf{z}}} \quad \phi, \sigma \in [0, 2\pi), \psi \in [0, \pi] \tag{2}$$

The 2-DoF *tilt motion* $e^{\psi \widehat{\mathbf{w}}}$, with $\mathbf{w} = c_\phi \mathbf{x} + s_\phi \mathbf{y}$, $\mathbf{x} = (1,0,0)^T$ and $\mathbf{y} = (0,1,0)^T$, unambiguously determines the configuration of the revolute axis $\mathbf{z}$ via:

$$\mathbf{R} \cdot \mathbf{z} = e^{\psi \widehat{\mathbf{w}}} e^{\sigma \widehat{\mathbf{z}}} \cdot \mathbf{z} = e^{\psi \widehat{\mathbf{w}}} \cdot \mathbf{z} \tag{3}$$

thereby defining a 2D (non-redundant) motion manifold:

$$\begin{aligned} \mathrm{M} &:= \left\{ e^{\psi(c_\phi \widehat{\mathbf{x}} + s_\phi \widehat{\mathbf{y}})} \;\middle|\; \phi \in [0, 2\pi), \psi \in [0, \pi] \right\} \\ &= \exp\{\widehat{\mathbf{x}}, \widehat{\mathbf{y}}\}_{\mathrm{span}} \end{aligned} \tag{4}$$

It is also the set of all unit quaternions $(q_0, q_x, q_y, q_z) \in \mathbb{R}^4$ with $q_z = 0$ [11,12].

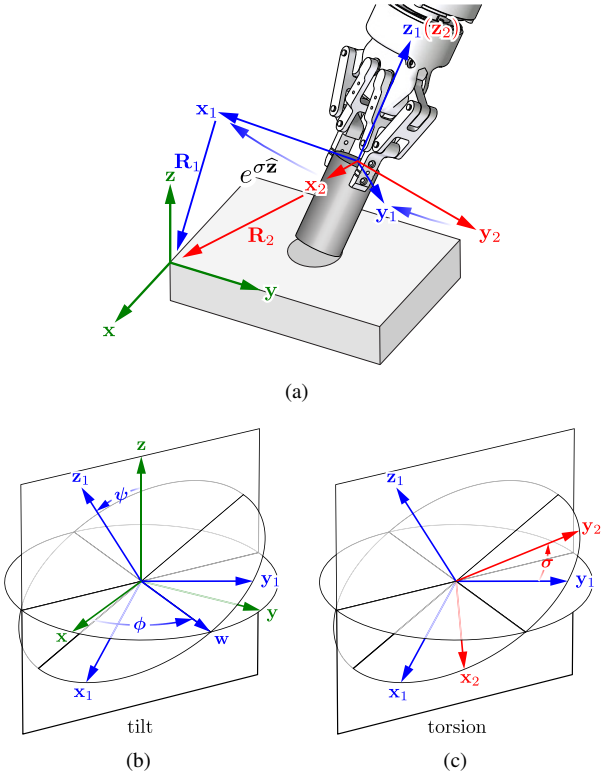

Fig. 1. (a) Orientation ambiguity in peg-in-hole task; (b) and (c) a tilt-torsion characterization of the ambiguity.

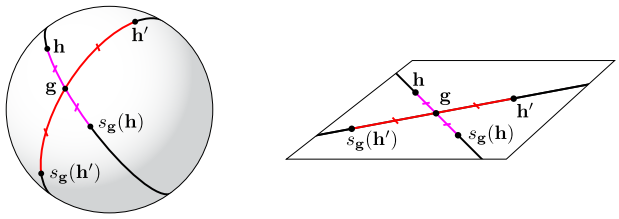

Fig. 2. Examples of symmetric spaces and their associated inversion symmetry on (a) the unit 2-sphere S^2 (geodesics are great circles); and (b) the Euclidean plane $\mathbb{R}^2$ (geodesics are straight lines).

Recently, we pointed out in [13] that the manifold M in Eq. (4) admits the structure of a *symmetric subspace* (SS) of $\mathrm{SO}(3)$ and, hence, of $\mathrm{SE}(3)$. Indeed, $\mathrm{SE}(3)$ is a *symmetric space* [14] with an involutive automorphism $s_{\mathbf{g}}$ (i.e., $s_{\mathbf{g}} \circ s_{\mathbf{g}} = id_{\mathrm{SE}(3)}$), called *inversion symmetry*, defined at each point $\mathbf{g} \in \mathrm{SE}(3)$:

$$s_{\mathbf{g}}(\mathbf{h}) := \mathbf{g}\mathbf{h}^{-1}\mathbf{g} \quad \forall \mathbf{h} \in \mathrm{SE}(3) \tag{5}$$

which generalizes the concept of geodesic reflection on a unit 2-sphere S^2 or a Euclidean plane $\mathbb{R}^2$, as illustrated in Fig. 2 [1]. A SS M, such that defined in Eq. (4), is always generated by the exponential image of a *Lie triple subsystem* (LTS) $\mathfrak{m}$ of $\mathfrak{se}(3)$ (i.e., a vector subspace $\mathfrak{m}$ satisfying closure under double commutators $[[\mathfrak{m},\mathfrak{m}],\mathfrak{m}] \subset \mathfrak{m}$):

$$\mathrm{M} = \exp \mathfrak{m} \tag{6}$$

[1]Strictly speaking, a nD Euclidean space is an affine space [15], which is equivalent to $\mathbb{R}^n$ when a particular reference coordinate frame is chosen. The choice of the reference frame is irrelevant, for the purpose of this paper.

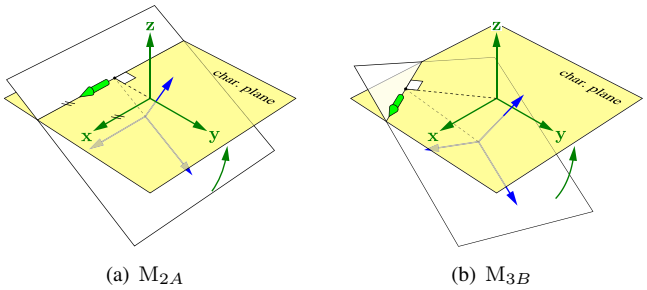

Fig. 3. Manipulation with plane symmetry: (a) the 1T1R SS M_{2A} characterizes tilting of its LTS plane about any screw axis in $\mathfrak{m}_{2A}$ (a parallel pencil of 0-pitch screws lying on and a ∞-pitch screw perpendicular to the LTS characteristic plane); (b) the 1T2R SS M_{3B} characterizes tilting of its characteristic plane about any screw axis in $\mathfrak{m}_{3B}$ (a planar field of 0-pitch screws lying on and a ∞-pitch screw perpendicular to the characteristic plane).

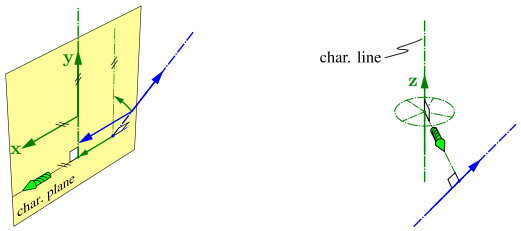

Fig. 4. Manipulation with line symmetry: (a) the 2T1R SS M_{3A} characterizes the displacement of a line (the $\mathbf{y}$-axis) that perpendicularly intersects all screws in $\mathfrak{m}_{3A}$ while maintaining it perpendicular to the $\mathbf{x}$-axis; (b) the 2T2R SS M_4 characterizes the displacement of its characteristic line (the $\mathbf{z}$-axis) to an arbitrary location.

Following this lead, we provided a complete classification of LTSs of $\mathfrak{se}(3)$ along with their associated SSs of $\mathrm{SE}(3)$ in [12,13]. We denote a mD SS with one and two rotational DoFs by M_{mA} and M_{mB} respectively; their corresponding LTSs are $\mathfrak{m}_{mA}$ and $\mathfrak{m}_{mB}$, respectively. M_{4B} and M_{5B} are simply denoted by M_4 and M_5, since M_{4A} and M_{5A} do not exist. Thus, for example, the SS in Eq. (4) is denoted by M_{2B}, and its LTS $\{\widehat{\mathbf{x}}, \widehat{\mathbf{y}}\}_{\mathrm{span}}$ is $\mathfrak{m}_{2B}$. We also identified the decomposition of Eq. (2) as a special case of the parametrization of the *completion group* G_{M} of M by the Cartesian product of $\mathfrak{m}$ and its *commutator algebra* $\mathfrak{h}_{\mathfrak{m}} := [\mathfrak{m},\mathfrak{m}]$:

$$\begin{aligned} \widetilde{\exp} : \mathfrak{m} \times \mathfrak{h}_{\mathfrak{m}} &\to \mathrm{G}_{\mathrm{M}} \\ (\boldsymbol{\xi}, \boldsymbol{\eta}) &\mapsto e^{\boldsymbol{\xi}} e^{\boldsymbol{\eta}} \ (\text{or } e^{\boldsymbol{\eta}} e^{\boldsymbol{\xi}}) \end{aligned} \tag{7}$$

which is also referred to as a *generalized polar decomposition* (GPD) [16].

We investigated in [17] several advantages of M_{2B} by drawing on the theory of submanifolds [18]: M comprises shortest rotation paths between the initial configuration $\mathbf{z}$ and a generic configuration $\mathbf{R}\mathbf{z}$; M_{2B} has exactly the same expressions for acceleration as $\mathrm{SO}(3)$. Indeed, M_{2B} underlies the human eye saccade movement [19,20], and in some sense provides an optimal redundancy resolution for 2D orienting.

Our preliminary results in [13,17] may be systematically generalized to characterize motion manifolds of objects with plane and line symmetry [21] by resorting to higher dimensional SSs of $\mathrm{SE}(3)$. For example, 1-translational-1-rotational

(1T1R [2]) or 1T2R motion modules of planar or spatial hyper-redundant robots [22]–[24], due to their physical construction, often generate plane symmetric motions, as illustrated in Fig. 3; Renda *et al.* also suggested its application in modeling locally plane symmetric continuum robots [25]. Line symmetric motions, as illustrated in Fig. 4, can be naturally associated with the 1T2R (planar) or 2T2R (spatial) task of positioning a needle or laparoscope for minimal invasive surgery [26]. Finally, wearable exoskeleton for robotic rehabilitation [27]–[31] often requires passively or actively aligning robot and human joint axes, which involve all three types of symmetry. We shall refer to the aforementioned motion tasks as *symmetric manipulation* tasks.

Despite the aforesaid advantages of SSs for portraying symmetric manipulation tasks outside the Lie group framework, there is no theory or methodology available for the systematic synthesis of their motion generators. Indeed, in mechanism synthesis community, mixed DoFs such as 1T2R and 2T2R DoFs are almost always associated with *product-of-exponentials submanifolds* (POEs), i.e., the motion manifolds generated by serial kinematic chains [32]–[35]. Unlike SSs, POEs in general introduce undesired redundant motions and therefore are not ideal motion generators for symmetric manipulation tasks. To fully explore SS motion manifolds in symmetric manipulation, in this paper we develop a systematic type synthesis method for SS motion generators. Our work is motivated by the fact that the SS synthesis problem is essentially different from those solvable by state-of-the-art type synthesis methods [32,34,36]–[38]. Notable exceptions include some efforts towards the synthesis of M_{3B}-PMs [39,40].

B. Related works

Popplestone *et al.* used Lie subgroups of $\mathrm{SE}(3)$ to study assembly planning of objects with symmetry [7]. Li *et al.* used homogeneous space to model the configuration space of symmetric objects for workpiece localization algorithms [8] and robot kinematic calibration [41]. Discrete symmetry groups are investigated in computer vision [42,43].

Hervé *et al.* initiated research on type synthesis of parallel manipulators (PMs) using Lie subgroups [1,44] and dependent products (of Lie subgroups) of $\mathrm{SE}(3)$ [32,38]. Both Lie subgroups and dependent products can be represented by POEs [33,45]. Meanwhile, Hunt [39] initiated type synthesis of PM using screw theory of $\mathfrak{se}(3)$, which is later pursued by Carricato *et al.* [35,37,40,46,47], Huang, Li *et al.* [32,36,48], Fang, Tsai *et al.* [49,50], Kong, Gosselin *et al.* [51]–[53], etc.

Bonev *et al.* proposed a tilt-torsion parametrization of $\mathrm{SO}(3)$ for characterizing the orientation workspace of PMs [10], and later investigated zero-torsion PMs [54]. In particular, homokinetic-coupling-equivalent PMs [39,40] are zero-torsion PMs. Later, we showed that the motion manifolds of both 2R and 1T2R homokinetic-coupling-equivalent PMs are given by the exponential image of LTSs of $\mathfrak{se}(3)$ (and therefore are SSs of $\mathrm{SE}(3)$), which prompted us to systematically investigate SSs of $\mathrm{SE}(3)$ [13].

Aside from Lie subgroups, which are trivially SSs, a total of seven conjugacy classes of SSs of $\mathrm{SE}(3)$ are reported in [13]. We also presented ample evidence that SSs are suitable motion manifolds for analyzing various mechanical / kinesiological systems. Selig used LTSs and Cartan decomposition to investigate a class of explicitly solvable optimal motion planning problem [55]. The role of symmetric space and GPD in numerical integration and interpolation is investigated by Munthe-Kass [16] and Gawlik and Leok [56]. The SSs of $\mathrm{SE}(3)$ and their symmetric twist pairs are reported in Appendix B for convenience of the reader.

C. Organization of the paper

The paper is organized as follows. In Section II, we give a brief review of state-of-the-art PM type synthesis method with an emphasis on SSs. We prove that not all SSs admit PM realization. To break this limitation, in Section III we propose a systematic type synthesis method for SS motion generators with general topology. We classify SSs into three overlapping subcategories according to their synthesizability under different topology assumptions:

A) $\mathrm{M}_{2A}, \mathrm{M}_{2B}$ and M_{3B} admit PM realizations;
B) all SSs except M_5 admit *inter-connected* PMs (ICPMs);
C) M_{3A} and M_5 admit *serial-parallel hybrid manipulators* (SPHMs).

For each subcategory, a number of exemplifying manipulators are presented. In Section IV, we show how the synthesized SS motion generators may be use to manipulate objects with revolute, plane or line symmetry, along with a discussion about their potential application in robotics.

II. PM Type Synthesis for Symmetric Subspaces

From a motion manifold viewpoint, the many state-of-the-art PM type synthesis methods summarized in Sec. I-B are equivalent to the following procedure:

***Procedure* 1** : type synthesis of PMs**.**

1) ***Initialization:*** *specify* M *as the desired motion manifold of the PM to be synthesized.*
2) ***Chain synthesis:*** *synthesize chains* $\mathcal{M}_i$*'s with motion manifolds* M_i*'s such that* M_i *contains* M *(in a neighborhood of* $\mathbf{I}$*):*
$$\mathrm{M} \subset \mathrm{M}_i \tag{8}$$
The joint twists in a chain should be linearly independent to avoid internal motion.
3) ***PM synthesis:*** *select from all admissible chains synthesized in 1) a combination of* l *chains* $\mathcal{M}_i, i = 1, ..., l$ *with motion manifolds* M_1*,...,*M_l*, such that* $\bigcap_{i=1}^{l} \mathrm{M}_i$ *and* M *are equal (in a neighborhood of* $\mathbf{I}$*):*
$$\bigcap_{i=1}^{l} \mathrm{M}_i = \mathrm{M} \tag{9}$$
4) ***End***. □

The issue of actuation selection is not essential for the development of our paper and is therefore not included in the above procedure.

[2]The notion of $m\mathrm{T}n\mathrm{R}$ motion, although widely used in mechanisms and robotics research, does not accurately define a unique motion manifold. In this paper, such a notion merely serves as a quick reference to predefined motion manifolds, such as Lie subgroups and symmetric subspaces listed in Tab. B.1.

If Eq. (8) is satisfied for all motion manifolds M_i's, Eq. (9) may conveniently be replaced by:

$$\textstyle\bigcap_{i=1}^{l} S_i = S \tag{9a}$$

where $S_i := \mathrm{T}_{\mathbf{I}}\mathrm{M}_i, i = 1, ..., l$ and $S := \mathrm{T}_{\mathbf{I}}\mathrm{M}$, or dually,

$$\textstyle\sum_{i=1}^{l} S_i^{\perp} = S^{\perp} \tag{9b}$$

where $S_i^{\perp}$ and $S^{\perp}$ denote the *annihilator*s or the constraint wrench spaces of S and S_i, respectively:

$$\begin{aligned} S_i^{\perp} &:= \left\{ \boldsymbol{\zeta} \in \mathfrak{se}(3)^* \mid \boldsymbol{\zeta}^T \cdot \boldsymbol{\xi} = 0,\ \forall \boldsymbol{\xi} \in S_i \right\} \\ S^{\perp} &:= \left\{ \boldsymbol{\zeta} \in \mathfrak{se}(3)^* \mid \boldsymbol{\zeta}^T \cdot \boldsymbol{\xi} = 0,\ \forall \boldsymbol{\xi} \in S \right\} \end{aligned} \tag{10}$$

where $\mathfrak{se}(3)^*$ is the dual space of $\mathfrak{se}(3)$, $\boldsymbol{\zeta}$ is a wrench expressed in ray coordinates and $\boldsymbol{\xi}$ is a twist expressed in axis coordinates.

Equation (9b) is often referred to as the *constraint synthesis condition* (CSC) [36]. The equivalence of Eq. (9a) or Eq. (9b) to Eq. (9) is essentially due to the following fact. The rank of the constraint Jacobian matrix, i.e., the number of its non-zero singular values, cannot decrease by small perturbations, whereas Eq. (8) ensures that the rank cannot increase either. A detailed proof can be found in [33, Prop. 6].

A. Chain synthesis for symmetric subspace motion generators

Without loss of generality, we restrict ourselves to 1-DoF Reuleaux lower pairs for serial chain synthesis. The chain motion manifold M_i will therefore always be a POE $\prod_{j=1}^{k_i} \exp\{\boldsymbol{\xi}_{ij}\}_{\mathrm{span}}$, with $k_i = \dim \mathrm{M}_i$ and $\boldsymbol{\xi}_{ij}$ the j-th joint twist. We also assume that the joint twists in a chain are linearly independent.

Note that the POE generated by any basis of a kD LTS $\mathfrak{m}$, namely $\prod_{j=1} \exp\{\boldsymbol{\xi}_j\}_{\mathrm{span}}$ with $\{\boldsymbol{\xi}_1, ..., \boldsymbol{\xi}_k\}_{\mathrm{span}} = \mathfrak{m}$, is not equal to the corresponding SS M (see Appendix D for a rigorous proof). In other words, the GPD of a generic configuration of $\prod_{j=1}^{k} \exp\{\boldsymbol{\xi}_j\}_{\mathrm{span}}$:

$$e^{\theta_1 \boldsymbol{\xi}_1} ... e^{\theta_k \boldsymbol{\xi}_k} = e^{\boldsymbol{\xi}} e^{\boldsymbol{\eta}} \qquad \boldsymbol{\xi} \in \mathfrak{m},\ \boldsymbol{\eta} \in \mathfrak{h}_{\mathfrak{m}} \tag{11}$$

will have a non-trivial H_{M}-component $e^{\boldsymbol{\eta}}$, i.e., $\boldsymbol{\eta} \neq \mathbf{0}$. The concept of *symmetric twist pair* (SP) and *symmetric twist chain* (SC) introduced in our earlier work [13] are essentially means of eliminating the H_{M}-component from Eq. (11), which we briefly review as follows.

Review : *symmetric pair and symmetric chain [13]. Given a kD SS M with LTS $\mathfrak{m}$, a SP of type $\mathfrak{m}$, denoted $\mathfrak{m}$-SP, is an ordered pair of twists $(\boldsymbol{\xi}^+, \boldsymbol{\xi}^-)$ with $\boldsymbol{\xi}^+, \boldsymbol{\xi}^- \in \mathfrak{g}_{\mathfrak{m}}$ that admit the following condition:*

$$\begin{cases} \boldsymbol{\xi}^+ = \boldsymbol{\xi} + \boldsymbol{\eta} \\ \boldsymbol{\xi}^- = \boldsymbol{\xi} - \boldsymbol{\eta} \end{cases} \qquad \boldsymbol{\xi} \in \mathfrak{m}, \boldsymbol{\eta} \in \mathfrak{h}_{\mathfrak{m}} \tag{12}$$

Geometrically, the axes of $(\boldsymbol{\xi}^+, \boldsymbol{\xi}^-)$ attain symmetry about either a characteristic plane that contains the screws of $\mathfrak{m}$ (for $\mathrm{M}_{2A}, \mathrm{M}_{2B}, \mathrm{M}_{3A}$ and M_{3B}) or a characteristic line that perpendicularly intersects the screws of $\mathfrak{m}$ (for M_4).

A SC of type $\mathfrak{m}$, denoted $\mathfrak{m}$-SC, is a kinematic chain $\mathcal{M}_i$ (i being the leg index) with k nesting $\mathfrak{m}$-SPs $(\boldsymbol{\xi}_{ij}^+, \boldsymbol{\xi}_{ij}^-)$, $j = 1, ..., k$:

$$\mathcal{M}_i := (\boldsymbol{\xi}_{i1}^+, ..., \boldsymbol{\xi}_{ik}^+, \boldsymbol{\xi}_{ik}^-, ..., \boldsymbol{\xi}_{i1}^-) \tag{13}$$

such that $\boldsymbol{\xi}_{ij}^{\pm} = \boldsymbol{\xi}_{ij} \pm \boldsymbol{\eta}_{ij}$, $\boldsymbol{\xi}_{ij} \in \mathfrak{m}$, $\boldsymbol{\eta}_{ij} \in \mathfrak{h}_{\mathfrak{m}}$, $j = 1, ..., k$ and satisfy

$$\{\boldsymbol{\xi}_{i1}, ..., \boldsymbol{\xi}_{ik}\}_{\mathrm{span}} = \mathfrak{m} \tag{14a}$$

When $\mathfrak{m} \cap \mathfrak{h}_{\mathfrak{m}} = \mathbf{0}$ (i.e., $\mathfrak{m} \neq \mathfrak{m}_5$), condition Eq. (14a) is equivalent to either one of the following two conditions:

$$\{\boldsymbol{\xi}_{i1}^+, ..., \boldsymbol{\xi}_{ik}^+\}_{\mathrm{span}} \oplus \mathfrak{h}_{\mathfrak{m}} = \mathfrak{g}_{\mathfrak{m}} \tag{14b}$$

$$\{\boldsymbol{\xi}_{i1}^-, ..., \boldsymbol{\xi}_{ik}^-\}_{\mathrm{span}} \oplus \mathfrak{h}_{\mathfrak{m}} = \mathfrak{g}_{\mathfrak{m}} \tag{14c}$$

We shall refer to $(\boldsymbol{\xi}_{i1}^+, ..., \boldsymbol{\xi}_{ik}^+)$ and $(\boldsymbol{\xi}_{ik}^-, ..., \boldsymbol{\xi}_{i1}^-)$ as the proximal *and* distal half *of the SC, which we denote by $\mathcal{M}_i^+$ and $\mathcal{M}_i^-$, respectively. Their motion manifolds will be denoted by M_i^+ and M_i^- respectively. Note also that a $\mathfrak{m}$-SC may have either $2k$ or $2k-1$ joints, with the latter occurring when $\boldsymbol{\xi}_{ik}^+ = \boldsymbol{\xi}_{ik}^-$ or equivalently $\boldsymbol{\eta}_{ik} = \mathbf{0}$, so that the innermost SP $(\boldsymbol{\xi}_{ik}^+, \boldsymbol{\xi}_{ik}^-)$ collapses into a single joint $\boldsymbol{\xi}_{ik}$. We shall refer to the SC with $2k$ and $2k-1$ joints as* even *SC and* odd *SC, respectively.* □

Since all joint twists in a $\mathfrak{m}$-SC $\mathcal{M}_i$ are members of the completion algebra $\mathfrak{g}_{\mathfrak{m}}$ of $\mathfrak{m}$, the chain motion manifold $\mathrm{M}_i^+ \cdot \mathrm{M}_i^-$ is either a submanifold of, or equal to, the completion group G_{M}. In the former case, since

$$\begin{aligned} \mathrm{M}_i^+ \cdot \mathrm{M}_i^- &= \left\{ \textstyle\prod_{j=1}^{k} e^{\theta_{ij}^+ \boldsymbol{\xi}_{ij}^+} \prod_{j=k}^{1} e^{\theta_{ij}^- \boldsymbol{\xi}_{ij}^-} \;\middle|\; \theta_{ij}^{\pm} \in \mathbb{R} \right\} \\ \mathrm{M} &= \left\{ \textstyle\prod_{j=1}^{k} e^{\theta_{ij} \boldsymbol{\xi}_{ij}^+} \prod_{j=k}^{1} e^{\theta_{ij} \boldsymbol{\xi}_{ij}^-} \;\middle|\; \theta_{ij} \in \mathbb{R} \right\} \end{aligned} \tag{15}$$

the chain synthesis condition $\mathrm{M} \subset (\mathrm{M}_i^+ \cdot \mathrm{M}_i^-)$ is satisfied. We say that M is generated by $\mathcal{M}$ under the *symmetric movement condition* (SMC):

$$\theta_{ij}^+ \equiv \theta_{ij}^- \qquad i = 1, ..., l, j = 1, ..., k \tag{16}$$

In the latter case, the $\mathfrak{m}$-SC can be effectively replaced by any $\mathfrak{g}_{\mathfrak{m}}$-chain irrespective of the SMC.

B. PM synthesis for M_{2A}, M_{2B} and M_{3B}

A PM comprising multiple $\mathfrak{m}$-SCs generates the corresponding SS $\mathrm{M} = \exp \mathfrak{m}$ if the CSC Eq. (9b) is satisfied.

For example, a typical M_{3B}-PM, also known as the 3-$\mathcal{RSR}$ (or 3-5$\mathcal{R}$) PM or the reflected tripod [40,54,57], is shown in Fig. 5(c). The end-effector of this mechanism may perform either a *finite* rotation about any axis lying in, or a *finite* translation along the normal to, the characteristic plane as shown in Fig. 5(a). Its three chains $\mathcal{M}_1$, $\mathcal{M}_2$ and $\mathcal{M}_3$ are rendered in light brown, cyan and pink respectively, and are all odd $\mathfrak{m}_{3B}$-SCs generated from $\mathfrak{m}_{3B}$-SPs, as shown in Fig. 5(b). Since each chain admits only one independent constraint wrench $\boldsymbol{\zeta}_i, i = 1, 2, 3$, as shown in Fig. 5(d), the CSC Eq. (9b) is given by:

$$\textstyle\sum_{i=1}^{3} S_i^{\perp} = \{\boldsymbol{\zeta}_1, \boldsymbol{\zeta}_2, \boldsymbol{\zeta}_3\}_{\mathrm{span}} = \mathfrak{m}_{3B}^{\perp} \tag{17}$$

Recall that the *screw system* [3] of $\mathfrak{m}_{3B}$, shown in Fig. 5(a), comprises a planar field of 0-pitch screws along with an ∞-pitch screw perpendicular to it; it is also self-reciprocal [57],

[3]Following the convention of [57], a system of $n, n \leq 6$, linearly independent twists span a nD vector subspace of the Lie algebra $\mathfrak{se}(3)$; its associated screw system is the corresponding $(n-1)$D projective subspace of a 5D real projective space $\mathbb{R}\mathrm{P}^5$ (ignoring the magnitude of the screw). This screw system is usually called a n-system.

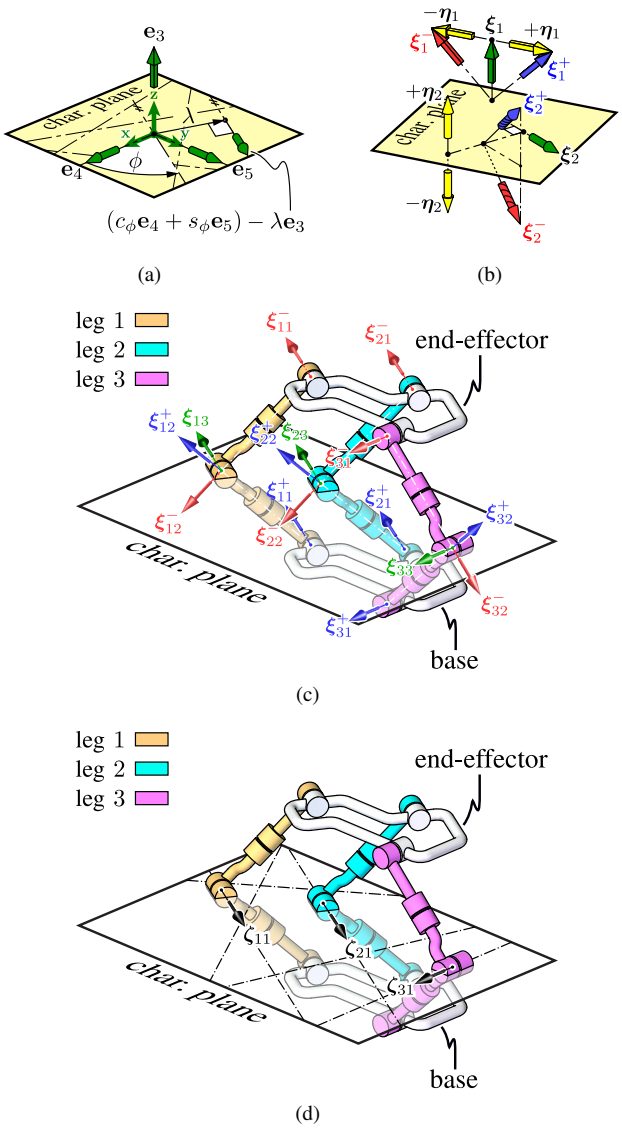

Fig. 5. Example of a M_{3B}-PM comprising three $5\mathcal{R}$ (in a $\mathcal{RSR}$ configuration) $\mathfrak{m}_{3B}$-SCs, which are all mirror symmetric about a common characteristic plane (reflected tripod [57]). (a) screw system of $\mathfrak{m}_{3B}$; (b) various examples of $\mathfrak{m}_{3B}$-SPs (green arrow: screw in $\mathfrak{m}_{3B}$; yellow arrow: screw in $\mathfrak{h}_{3B}$; red / blue arrow pair: SP); (c) joint twists of the PM; (d) constraint wrenches.

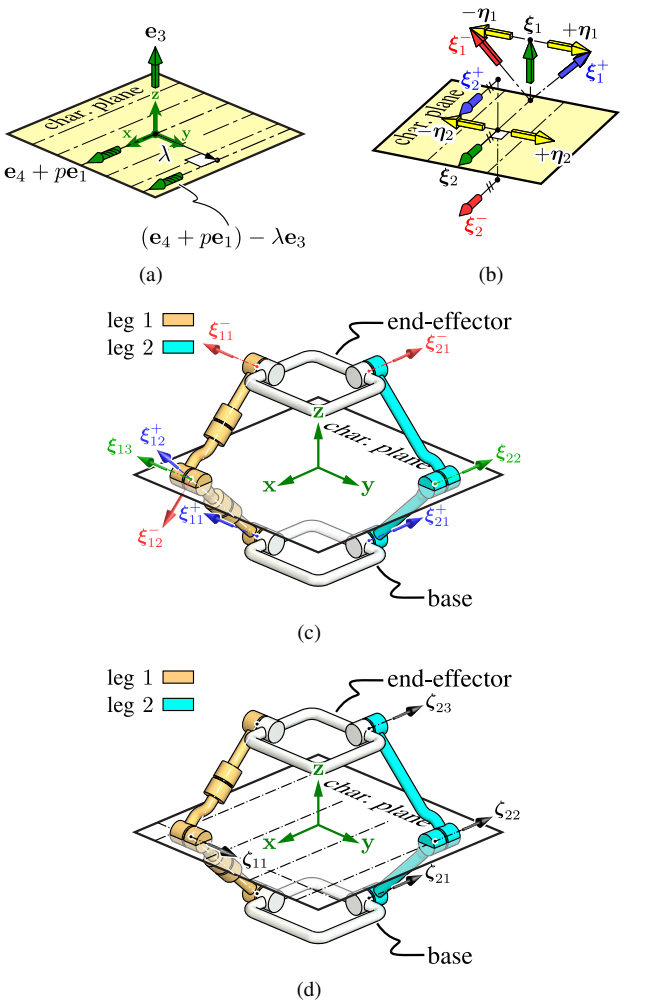

Fig. 6. Example of a M_{2A}-PM comprising a mirror symmetric $5\mathcal{R}$ $\mathfrak{m}_{3B}$-SC and a planar chain, whose planar normal is parallel to the characteristic plane of the former. (a) screw system of $\mathfrak{m}^p_{2A}$ ($\mathfrak{m}_{2A}$ if $p = 0$); (b) various examples of $\mathfrak{m}_{2A}$-SPs; (c) joint twists of the PM; (d) constraint wrenches.

meaning the constraint wrench space $\mathfrak{m}^\perp_{3B}$ has the same screw system as $\mathfrak{m}_{3B}$. The CSC requires that the three lines representing the three constraint wrenches $\boldsymbol{\zeta}_i$'s, $i = 1, 2, 3$, must be neither mutually concurrent nor parallel. This synthesis condition first appeared in [39] and was later revisited in [54] and in [40].

We emphasize that the SCs of a kD LTS $\mathfrak{m}$ in a SS-PM must have either $2k - 1$ (odd SC) or $2k$ (even SC) linearly independent (and hence no more than six) joint twists according to Procedure 1; since no more than 6 twists can be linearly independent, k must be smaller than or equal to 3. For example, any SC of $\mathfrak{m}_4$ (resp., $\mathfrak{m}_5$) comprises at least seven (resp., nine) joint twists and does not serve as legitimate chains for PM synthesis.

Another restraint comes from the fact that when only Lie subgroup chains (say, generating a Lie subgroup $\mathrm{G}_i, i = 1, ..., l$) are employed, the resulting PM necessarily has a Lie subgroup motion manifold $\cap_{i=1}^{l} \mathrm{G}_i$ instead of the desired SS. For example, it can be verified that $\mathfrak{m}_{2A}$-SCs (resp., $\mathfrak{m}_{2B}$-SCs and $\mathfrak{m}_{3A}$-SCs) are necessarily $\mathfrak{g}_{2A}$-chains (resp., $\mathfrak{g}_{2B}$-chains and $\mathfrak{g}_{3A}$-chains). Consequently, one can not synthesize M_{2A}-PMs, M_{2B}-PMs or M_{3A}-PMs with only their corresponding SCs.

On the other hand, since $\mathfrak{m}_{3B}$ is a parent LTS of $\mathfrak{m}_{2A}$ and $\mathfrak{m}_{2B}$, a $\mathfrak{m}_{3B}$-SC necessarily satisfies the chain synthesis condition Eq. (8) for M_{2A} and M_{2B}, i.e., its chain motion manifold contains M_{2A} and M_{2B} respectively. A M_{2A}-PM (resp., M_{2B}-PM) may then be synthesized using a combination of $\mathfrak{m}_{3B}$-SCs and $\mathfrak{g}_{2A}$-chains (resp., $\mathfrak{g}_{2B}$-chains) as shown in Fig. 6(c) and Fig. 7(c) respectively. In both cases, all SCs in a synthesized PM must share the same characteristic plane.

To proceed with Procedure 1, we verify the CSC for the M_{2A}-PM shown in Fig. 6(c) as follows. Since the screw system of $\mathfrak{m}_{2A}$ comprises a parallel pencil of 0-pitch screws and an ∞-pitch screw perpendicular to the pencil plane (see Fig. 6(a)), its constraint wrench system comprises a four-system that may be spanned by $\mathfrak{g}^\perp_{2A}$ (spanned by $\boldsymbol{\zeta}_{21}, \boldsymbol{\zeta}_{22}$ and

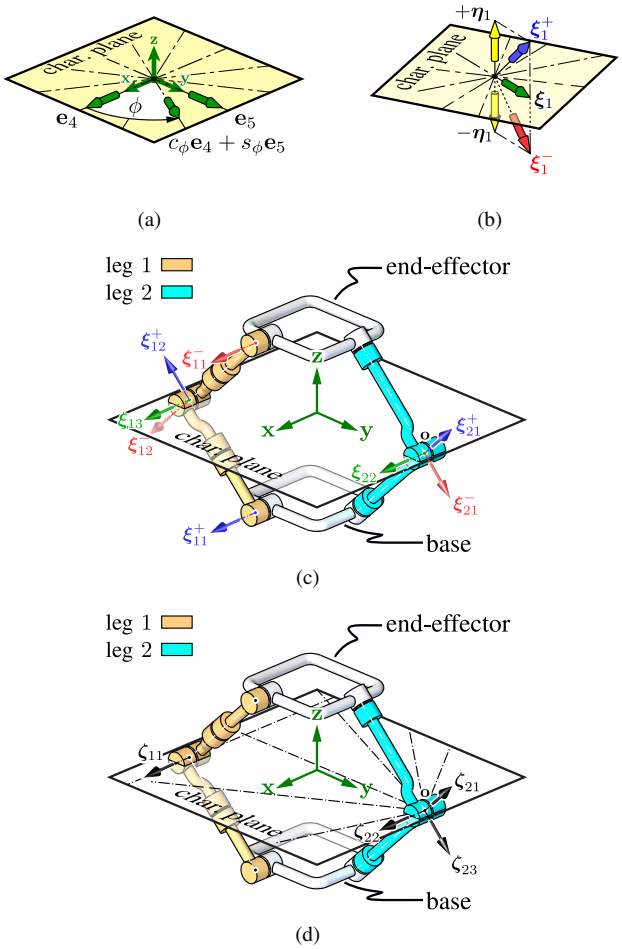

Fig. 7. Example of a M_{2B}-PM comprising a mirror symmetric $5\mathcal{R}$ $\mathfrak{m}_{3B}$-SC and a spherical chain, whose center of rotation $\mathbf{o}$ lies on the characteristic plane of the former. (a) screw system of $\mathfrak{m}_{2A}$; (b) various examples of $\mathfrak{m}_{2A}$-SPs; (c) joint twists of the PM; (d) constraint wrenches.

$\boldsymbol{\zeta}_{23}$ in Fig. 6(d)) and an additional 0-pitch wrench (e.g., $\boldsymbol{\zeta}_{11}$ in Fig. 6(d)) that intersects (not in-parallel) all twists in the pencil of $\mathfrak{m}_{2A}$:

$$S_1^\perp + \mathfrak{g}_{2A}^\perp = \mathfrak{m}_{2A}^\perp \tag{18}$$

In other words, by letting $\mathcal{M}_1 = (\boldsymbol{\xi}_{11}^+, \boldsymbol{\xi}_{12}^+, \boldsymbol{\xi}_{13}, \boldsymbol{\xi}_{12}^-, \boldsymbol{\xi}_{11}^-)$ be $\mathfrak{m}_{3B}$-SC and $\mathcal{M}_2 = (\boldsymbol{\xi}_{21}, \boldsymbol{\xi}_{22}, \boldsymbol{\xi}_{23})$ be a $\mathfrak{m}_{2A}$-SC (or more generally, a $\mathfrak{g}_{2A}$-chain, i.e., a 3-DoF planar chain), we may synthesize a M_{2A}-PM, as shown in Fig. 6(c), so long as: (i) the $\mathfrak{m}_{3B}$-SC $\mathcal{M}_1$ and the $\mathfrak{m}_{2A}$-SC $\mathcal{M}_2$ share the same characteristic plane, and (ii) the constraint force $\boldsymbol{\zeta}_1$ of $\mathcal{M}_1$ is not parallel to the constraint forces associated with $\mathfrak{m}_{2A}$ (see Fig. 6(d)). The end-effector of synthesized PM may perform *finite* rotation about any axis belonging to a parallel pencil prescribed by $\mathfrak{m}_{2A}$.

Similarly we may synthesize a M_{2B}-PM by letting $\mathcal{M}_1$ be the same $\mathfrak{m}_{3B}$-SC and $\mathcal{M}_2 = (\boldsymbol{\xi}_{21}, \boldsymbol{\xi}_{22}, \boldsymbol{\xi}_{23})$ be a $\mathfrak{m}_{2B}$-SC (or more generally, any $\mathfrak{g}_{2B}$-chain, i.e., a 3-DoF spherical chain), as shown in Fig. 7(c), so long as:

$$S_1^\perp + \mathfrak{g}_{2B}^\perp = \mathfrak{m}_{2B}^\perp \tag{19}$$

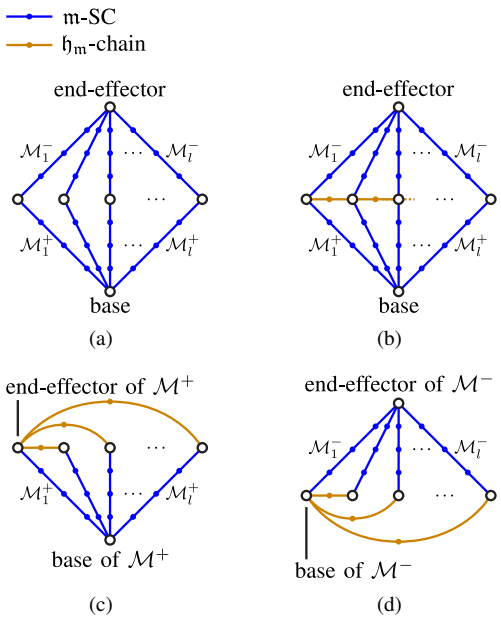

Fig. 8. Connectivity graph of an SS-ICPM generating a SS M other than M_5. (a) M-PM; (b) M-ICPM; (c) proximal half PM $\mathcal{M}^+$; (d) distal half PM $\mathcal{M}^-$.

or, equivalently, (i) the $\mathfrak{m}_{3B}$-SC $\mathcal{M}_1$ and $\mathfrak{m}_{2B}$-SC $\mathcal{M}_2$ share the same characteristic plane, and (ii) the constraint wrench $\boldsymbol{\zeta}_1$ of $\mathcal{M}_1$ does not pass through the center of the pencil of 0-pitch screws associated with $\mathfrak{m}_{2B}$ (Fig. 7(d)). This 2-DoF parallel wrist is a standard realization for 2-DoF constant-velocity (CV) couplings [39,40]. Its end-effector may perform *finite* rotation about any axis in the pencil prescribed by $\mathfrak{m}_{2B}$ (see Fig. 7(a)).

To summarize this section, we have shown that only $\mathrm{M}_{2A}, \mathrm{M}_{2B}$ and M_{3B} admit PM realizations. The PM type synthesis for M_{2B} and M_{3B} was systematically investigated by Hunt [39] and later by Carricato [40], without the knowledge of LTSs and SSs. The PM type synthesis for M_{2A} is performed here for the first time.

III. Type Synthesis of Symmetric Subspace Motion Generators with General Topology

We have shown in Sec. II-A that PM synthesis for SSs still revolves around traditional PM synthesis methods [33,34,36] with extensive use of SCs [13]. On the other hand, such synthesis results are limited to three out of seven SSs of $\mathrm{SE}(3)$, due to insufficient loop-closure constraints for the CSC Eq. (9b) (or equivalently the SMC in Eq. (16)). To compensate for the missing constraints, we may consider forming additional internal loops in a PM formed by multiple $\mathfrak{m}$-SCs, as illustrated by Fig. 8(a), so that the SMC of the $\mathfrak{m}$-SCs are not violated. It turns out that an effective and universal approach to accomplish this (for all SSs except M_5) is to impose an additional $\mathfrak{h}_\mathfrak{m}$-chain between the innermost links of each pair of $\mathfrak{m}$-SCs of the PM, as shown in Fig. 8(b), resulting in what we refer to as an inter-connected PM or ICPM [58].

A M-ICPM for a SS M other than M_5 may be essentially considered as two *intertwining* PMs which we call the *proximal half PM* and *distal half PM*, and denoted by $\mathcal{M}^+$ and

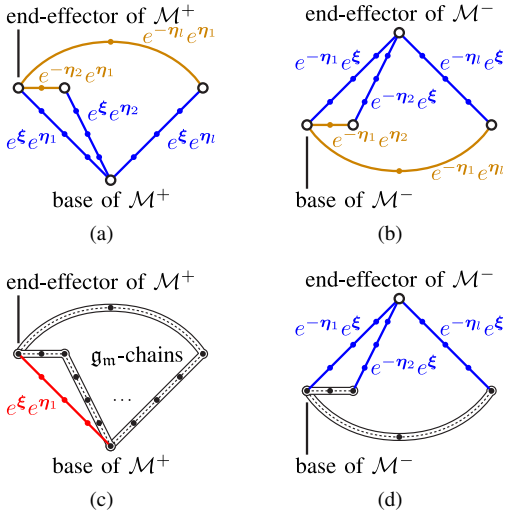

Fig. 9. GPD of the chain motions of a ICPM. (a) GPD of the proximal half PM $\mathcal{M}^+$; (b) GPD of the distal half PM $\mathcal{M}^-$ ($\mathcal{M}_1^+, \mathcal{M}_1^-$ obeying the SMC); (c) $\mathcal{M}^+$ after locking $\mathcal{M}_1^+$; (d) $\mathcal{M}^-$ after locking $\mathcal{M}_1^+$.

$\mathcal{M}^-$, respectively (see Fig. 8(c)). Without loss of generality, we specify that the base and end-effector of $\mathcal{M}^+$ are the base and the innermost link of the first leg of the ICPM, whereas the base and end-effector of $\mathcal{M}^-$ are the innermost link of the first leg and the end-effector of the ICPM. The word "intertwining" refers to the fact that $\mathcal{M}^+$ and $\mathcal{M}^-$ share the same interconnecting $\mathfrak{h}_\mathfrak{m}$-chains. Note that the same $\mathfrak{h}_\mathfrak{m}$-chain considered in $\mathcal{M}^+$ becomes its kinematic inverse in $\mathcal{M}^-$.

A. Type synthesis of SS-ICPMs for: M_{2A}, M_{2B}, M_{3A}, M_{3B} *and* M_4

Note from Fig. 8(c) that $\mathcal{M}_2^+, ..., \mathcal{M}_l^+$, when augmented with the interconnecting $\mathfrak{h}_\mathfrak{m}$-chains, become $\mathfrak{g}_\mathfrak{m}$-legs for $\mathcal{M}^+$. Their leg motion manifolds are thus, the completion group G_M, which contains the motion manifold M_1^+ of $\mathcal{M}_1^+$. Consequently, the motion of $\mathcal{M}^+$ is completely determined by that of $\mathcal{M}_1^+$. Similarly, the motion of $\mathcal{M}^-$ is completely determined by that of $\mathcal{M}_1^-$. The following theorem is the key to understanding the working principle of the ICPM.

***Theorem* 1.** *Given a* $\mathfrak{m}$*-SC* $\mathcal{M}_i = (\boldsymbol{\xi}_{i1}^+, ..., \boldsymbol{\xi}_{ik}^+, \boldsymbol{\xi}_{ik}^-, ..., \boldsymbol{\xi}_{i1}^-)$ *(*i *being leg index), with* $\mathfrak{m} \neq \mathfrak{m}_5$, $\dim \mathfrak{m} = k$ *and the following GPD for* M_i^+*:*

$$e^{\theta_{i1}\boldsymbol{\xi}_{i1}^+} ... e^{\theta_{ik}\boldsymbol{\xi}_{ik}^+} = e^{\boldsymbol{\xi}} e^{\boldsymbol{\eta}} \qquad \boldsymbol{\xi} \in \mathfrak{m}, \boldsymbol{\eta} \in \mathfrak{h}_\mathfrak{m} \tag{20}$$

where $\theta_{ij} \in (-\varepsilon, \varepsilon), j = 1, ..., k$ *for a sufficiently small positive number* $\varepsilon > 0$*, then we also have the following GPD for* M_i^-*:*

$$e^{\theta_{ik}\boldsymbol{\xi}_{ik}^-} ... e^{\theta_{i1}\boldsymbol{\xi}_{i1}^-} = e^{-\boldsymbol{\eta}} e^{\boldsymbol{\xi}} \tag{21}$$

Consequently,

$$e^{\theta_{i1}\boldsymbol{\xi}_{i1}^+} ... e^{\theta_{ik}\boldsymbol{\xi}_{ik}^+} e^{\theta_{ik}\boldsymbol{\xi}_{ik}^-} ... e^{\theta_{i1}\boldsymbol{\xi}_{i1}^-} = e^{\boldsymbol{\xi}} e^{\boldsymbol{\eta}} e^{-\boldsymbol{\eta}} e^{\boldsymbol{\xi}} = e^{2\boldsymbol{\xi}} \in \mathrm{M} \tag{22}$$

and $\mathcal{M}_i$ *generates* $\mathrm{M} = \exp \mathfrak{m}$ *under the SMC Eq.* (16) *if it satisfies one of the three equivalent conditions in Eq.* (14)*.*

Proof. See Appendix C. □

According to Theorem 1, the SMC of the ICPM is equivalent to a particular pattern of chain motions of the ICPM, as shown in Fig. 9 and elaborated as follows.

1) Given the GPD of a particular configuration of $\mathcal{M}_1^+$, say $e^{\boldsymbol{\xi}} e^{\boldsymbol{\eta}_1}, \boldsymbol{\xi} \in \mathfrak{m}, \boldsymbol{\eta}_1 \in \mathfrak{h}_\mathfrak{m}$, the GPD of $\mathcal{M}_1^-$ must be given by $e^{-\boldsymbol{\eta}_1} e^{\boldsymbol{\xi}}$, according to the SMC.
2) By the loop closure constraint of $\mathcal{M}^+$, as shown in Fig. 9(a), the GPD of $\mathcal{M}_i^+, i = 2, ..., l$ must be of the form $e^{\boldsymbol{\xi}} e^{\boldsymbol{\eta}_i}, \boldsymbol{\eta}_i \in \mathfrak{h}_\mathfrak{m}$. In other words, all $\mathcal{M}_i^+$'s should have the same M-component $e^{\boldsymbol{\xi}}$ while not necessarily having the same H_M-component $e^{\boldsymbol{\eta}_i}$'s.
3) The differences between the H_M-components $e^{\boldsymbol{\eta}_i}$'s are compensated by the $\mathfrak{h}_\mathfrak{m}$-chains (as subchains of $\mathcal{M}_+$), whose motion are then given by $e^{-\boldsymbol{\eta}_i} e^{\boldsymbol{\eta}_1}, i = 2, ..., l$.
4) By the same argument as in 2) and 3), the GPD of $\mathcal{M}_i^-$'s, $i = 1, ..., l$, under the SMC and loop closure constraint of $\mathcal{M}^-$ should be given by $e^{-\boldsymbol{\eta}_i} e^{\boldsymbol{\xi}}, i = 1, ..., l$, and the motion of the augmenting $\mathfrak{h}_\mathfrak{m}$-chains (as subchains of $\mathcal{M}_-$) are given by $e^{-\boldsymbol{\eta}_1} e^{\boldsymbol{\eta}_i}, i = 2, ..., l$, and they are exactly the inverse of the chain motions obtained in 3). This implies that imposing the $\mathfrak{h}_\mathfrak{m}$-chains does not violate the SMC of the ICPM.

The following arguments show that the SMC is the only possible motion of the ICPM.

5) All but the first leg of $\mathcal{M}^+$ are $\mathfrak{g}_\mathfrak{m}$-chains (each being a half $\mathfrak{m}$-SC $\mathcal{M}_i^+$ concatenated with a $\mathfrak{h}_\mathfrak{m}$-chain) with linearly independent joint twists. Therefore, the configuration of $\mathcal{M}^+$ is completely determined by that of $\mathcal{M}_1^+$. By fixing $\mathcal{M}_1^+$ at a desired configuration, each remaining leg of $\mathcal{M}^+$ becomes completely immobile (as indicated by a single solid link in Fig. 9(c) and (d)).
6) Consequently, if the remaining chains of $\mathcal{M}^-$ (as indicated by blue in Fig. 9(d)) are also immobile, i.e., if the PM formed by $\mathcal{M}_1^-, ..., \mathcal{M}_l^-$ becomes a structure, the ICPM will follow exactly the SMC for all full-cycle motion away from singularities.

The SMC along with the second half of Theorem 1 guarantees that the ICPM is a motion generator of the desired SS motion manifold M, which leads to the following procedure for synthesizing SS-ICPMs for a general SS $\mathrm{M} \neq \mathrm{M}_5$.

***Procedure* 2** : type synthesis of SS-ICPM*.*

1) **Initialization:** *Assign a SS* M *other than* M_5 *as motion manifold of the ICPM:* $\mathfrak{m} = \mathrm{T}_\mathbf{I}\mathrm{M}$, $\mathfrak{h}_\mathfrak{m} = [\mathfrak{m}, \mathfrak{m}]$, $\mathfrak{g}_\mathfrak{m} = \mathfrak{m} \oplus \mathfrak{h}_\mathfrak{m}$.

2) **SC synthesis:** *Synthesize, for the initial configuration, the distal half-SCs* $(\boldsymbol{\xi}_{ik}^-, ..., \boldsymbol{\xi}_{i1}^-)$, $i = 1, ..., l$, $k = \dim \mathfrak{m}$*, such that*

$$\underbrace{\{\boldsymbol{\xi}_{ik}^-, ..., \boldsymbol{\xi}_{i1}^-\}_\mathrm{span}}_{:= S_i^-} \oplus \mathfrak{h}_\mathfrak{m} = \mathfrak{g}_\mathfrak{m} \tag{23}$$

Then, synthesize the proximal half-SCs $(\boldsymbol{\xi}_{i1}^+, ..., \boldsymbol{\xi}_{ik}^+)$ *by the unique decomposition*

$$\begin{cases} \boldsymbol{\xi}_{ij}^+ = \boldsymbol{\xi}_{ij} + \boldsymbol{\eta}_{ij} \\ \boldsymbol{\xi}_{ij}^- = \boldsymbol{\xi}_{ij} - \boldsymbol{\eta}_{ij} \end{cases} \tag{24}$$

with $\boldsymbol{\xi}_{ij} \in \mathfrak{m}, \boldsymbol{\eta}_{ij} \in \mathfrak{h}_{\mathfrak{m}}$ *for* $i = 1, ..., l$ *and* $j = 1, ..., k$, *or equivalently by plane symmetry for* $\mathrm{M}_{2A}, \mathrm{M}_{2B}, \mathrm{M}_{3A}, \mathrm{M}_{3B}$ *or line symmetry for* M_4.

3) **Inter-SC chain synthesis:** *Synthesize inter-SC* $\mathfrak{h}_{\mathfrak{m}}$*-chains* $(\boldsymbol{\eta}_{m1}, ..., \boldsymbol{\eta}_{mh})$, $m = 2, ..., l$, $h = \dim \mathfrak{h}_{\mathfrak{m}}$, *such that:*

$$\{\boldsymbol{\eta}_{m1}, ..., \boldsymbol{\eta}_{mh}\}_{\text{span}} = \mathfrak{h}_{\mathfrak{m}} \tag{25}$$

4) **ICPM synthesis:** *verify that*

$$\sum_{i=1}^{l} (S_i^-)^{\perp} = \mathfrak{se}(3)^* \tag{26}$$

5) **End** ■

Remark. *Note that in Procedure 2, unlike in Procedure 1, we no longer require all twists* $\{\boldsymbol{\xi}_{i1}^+, ..., \boldsymbol{\xi}_{ik}^+; \boldsymbol{\xi}_{ik}^-, ..., \boldsymbol{\xi}_{i1}^-\}$, $k = \dim \mathfrak{m}$, *to be linearly independent. This offers many new design possibilities, even for SSs synthesizable by Procedure 1.* □

***Example* 1** : M_{2A}-ICPM and M_{2A}^p-ICPM. $\mathrm{M}_{2A} = \exp \mathfrak{m}_{2A} = \exp\{\mathbf{e}_3, \mathbf{e}_4\}_{\text{span}}$ comprises rotations about any axis in a planar parallel pencil and also a translation perpendicular to the pencil plane (see Fig. 6(a)). Consider now the synthesis of a M_{2A}-ICPM with l $3\mathcal{R}$ $\mathfrak{m}_{2A}$-SCs $(\boldsymbol{\xi}_{i1}^+, \boldsymbol{\xi}_{i2}, \boldsymbol{\xi}_{i1}^-)$, $i = 1, ..., l$. First, for *Step 2)* of Procedure 2, $\mathcal{M}_i^- = (\boldsymbol{\xi}_{i2}, \boldsymbol{\xi}_{i1}^-)$, $i = 1, ..., l$, should be designated in such a way that:

$$\{\boldsymbol{\xi}_{i2}, \boldsymbol{\xi}_{i1}^-\}_{\text{span}} \oplus \underbrace{\{\mathbf{e}_2\}_{\text{span}}}_{\mathfrak{h}_{2A}} = \underbrace{\{\mathbf{e}_2, \mathbf{e}_3, \mathbf{e}_4\}_{\text{span}}}_{\mathfrak{g}_{2A}} \tag{27}$$

Here, $\mathfrak{h}_{2A}$ is the 1D translation algebra along the $\mathbf{y}$-axis, and $\mathfrak{g}_{2A}$ is the 3D planar algebra on the $\mathbf{yz}$-plane. In other words, the plane passing through $\boldsymbol{\xi}_{i2}$ and $\boldsymbol{\xi}_{i1}^-$ should not be perpendicular to the characteristic plane of $\mathfrak{m}_{2A}$. This fully determines the l $\mathfrak{m}_{2A}$-SCs by plane symmetry.

Next, for *Step 3)*, since $\mathfrak{h}_{2A} = \{\mathbf{e}_2\}_{\text{span}}$, the inter-SC chains should each comprise only one prismatic joint along the $\mathbf{y}$-axis at the initial configuration (see yellow joints in Fig. 10).

Finally, for *Step 4)*, since the distal half PM (after locking the proximal half PM) $\mathcal{M}_1^- \| \cdots \| \mathcal{M}_l^-$ is a purely planar mechanism, each leg $\mathcal{M}_i^- = (\boldsymbol{\xi}_{i2}, \boldsymbol{\xi}_{i1}^-)$, $i = 1, ..., l$ contributes to one planar constraint force $\boldsymbol{\zeta}_{i1}$, as shown in Fig. 10(c). In order to satisfy Eq. (26), i.e.,

$$\{\boldsymbol{\zeta}_{11}, ..., \boldsymbol{\zeta}_{l1}\}_{\text{span}} + \mathfrak{g}_{2A}^{\perp} = \mathfrak{se}(3)^* \tag{28}$$

we need at least three $\mathfrak{m}_{2A}$-SCs for the M_{2A}-ICPM (rendered in light brown, cyan and pink in Fig. 10(a)), where $\boldsymbol{\zeta}_{11}, \boldsymbol{\zeta}_{21}$ and $\boldsymbol{\zeta}_{31}$ span a planar field of 0-pitch wrenches on the $\mathbf{yz}$-plane, as shown in Fig. 10(c).

For the synthesis of M_{2A}^p-ICPMs, note that the geometry of $\mathfrak{m}_{2A}$ and $\mathfrak{m}_{2A}^p$ is essentially the same. It is straightforward to verify that, by replacing all $\mathcal{R}$ joints in a M_{2A}-ICPM with $\mathcal{H}$ joints having a common pitch p, we obtain a corresponding M_{2A}^p-ICPM. One such example is shown in [59] without proof.

As we shall see in Sec. IV, a variant of the M_{2A}-ICPM may serve as an exoskeleton mechanism for the human elbow joint. □

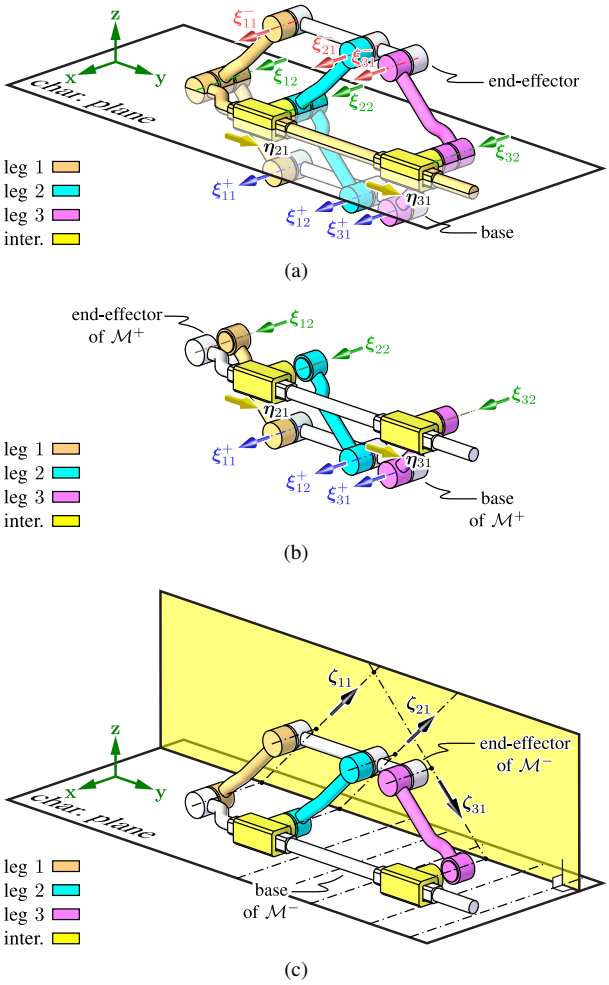

Fig. 10. Example of a M_{2A}-ICPM comprising three $3\mathcal{R}$ $\mathfrak{m}_{2A}$-SCs (with $\boldsymbol{\xi}_{i2}^+ = \boldsymbol{\xi}_{i2}^- = \boldsymbol{\xi}_{i2}$, $i = 1, 2, 3$). (a): joint twists of the ICPM; (b): proximal half PM; (c): distal half PM and constraint wrenches.

***Example* 2** : M_{2B}-ICPM. This design example was recently presented at ISRR2015 [60], where details of the theory were not shown. Consider the synthesis of an M_{2B}-ICPM as shown in Fig. 11. It comprises multiple $\mathfrak{m}_{2B}$-SCs , denoted by:

$$\mathcal{M}_i = (\boldsymbol{\xi}_{i1}^+, \boldsymbol{\xi}_{i2}, \boldsymbol{\xi}_{i1}^-), i = 1, ..., l. \tag{29}$$

where $\boldsymbol{\xi}_{i1}^+$, $\boldsymbol{\xi}_{i2}$ and $\boldsymbol{\xi}_{i1}^-$ are 0-pitch screws through $\mathbf{o}$, namely $(\mathbf{0}^{\mathrm{T}}, (\mathbf{w}_{i1}^+)^{\mathrm{T}})^{\mathrm{T}}$, $(\mathbf{0}^{\mathrm{T}}, \mathbf{w}_{i2}^{\mathrm{T}})^{\mathrm{T}}$ and $(\mathbf{0}^{\mathrm{T}}, (\mathbf{w}_{i1}^-)^{\mathrm{T}})^{\mathrm{T}}$, with $\mathbf{w}_{i1}^+$, $\mathbf{w}_{i2}$, $\mathbf{w}_{i1}^- \in \mathbb{R}^3$, respectively.

First, for *Step 2)* of Procedure 2, $\boldsymbol{\xi}_{i2}$ and $\boldsymbol{\xi}_{i1}^-$ should satisfy:

$$\{\boldsymbol{\xi}_{i2}, \boldsymbol{\xi}_{i1}^-\}_{\text{span}} \oplus \underbrace{\{\mathbf{e}_6\}_{\text{span}}}_{\mathfrak{h}_{2B}} = \underbrace{\{\mathbf{e}_4, \mathbf{e}_5, \mathbf{e}_6\}_{\text{span}}}_{\mathfrak{g}_{2B}} \tag{30}$$

for all $i = 1, ..., l$. In other words, the plane containing $\boldsymbol{\xi}_{i2}$ and $\boldsymbol{\xi}_{i1}^-$ should not be perpendicular to the characteristic plane (the $\mathbf{xy}$-plane at the initial configuration). This fully determines the l $\mathfrak{m}_{2B}$-SCs by plane symmetry.

Next, for *Step 3)*, since $\mathfrak{h}_{2B} = \{\mathbf{e}_6\}_{\text{span}}$, the inter-SC chains should each comprise only one revolute joint along the $\mathbf{z}$-axis at the initial configuration (see yellow links and joints in Fig. 11).

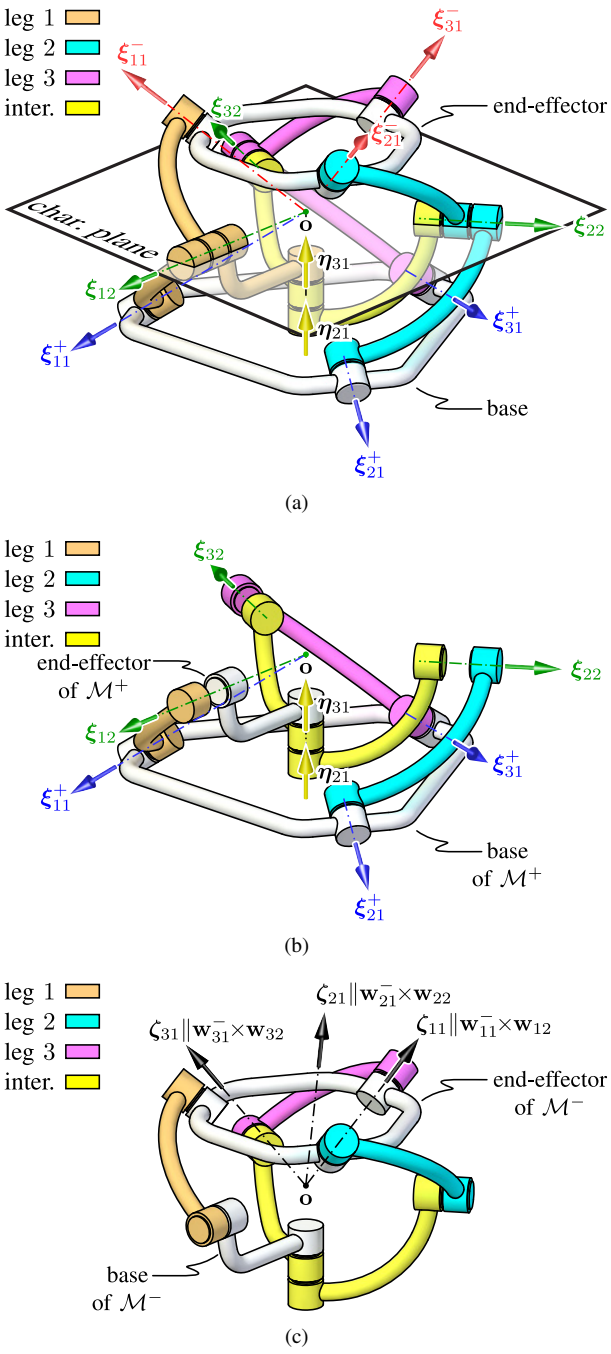

Fig. 11. Example of a M_{2B}-ICPM comprising three $3\mathcal{R}$ $\mathfrak{m}_{2B}$-SCs (with $\boldsymbol{\xi}_{i2}^+ = \boldsymbol{\xi}_{i2}^-$, $i = 1, 2, 3$). Inter-SC chains are rendered in yellow. (a) joint twists of the ICPM; (b) proximal half PM; (c) distal half PM and constraint wrenches.

Finally, for *Step 4)*, since the distal half PM (after locking the proximal half PM) $\mathcal{M}_1^- \| \cdots \| \mathcal{M}_l^-$ is a purely spherical mechanism, each leg $\mathcal{M}_i^- = (\boldsymbol{\xi}_{i2}, \boldsymbol{\xi}_{i1}^-), i = 1, ..., l$, contributes to one constraint torque $\boldsymbol{\zeta}_{i1}$ about $\mathbf{o}$, which is parallel to $\mathbf{w}_{i2} \times \mathbf{w}_{i1}^-$ (see Fig. 11(c)). In order to satisfy Eq. (26), i.e.,

$$\{\boldsymbol{\zeta}_{11}, ..., \boldsymbol{\zeta}_{l1}\}_{\text{span}} = \mathfrak{so}(3)^* \tag{31}$$

we need at least three $\mathfrak{m}_{2B}$-SCs for the M_{2B}-ICPM (rendered in light brown, cyan and pink in Fig. 11(a)), where $\boldsymbol{\zeta}_{11}, \boldsymbol{\zeta}_{21}$ and $\boldsymbol{\zeta}_{31}$ span a bundle of ∞-pitch screws, as shown in Fig. 11(c)).

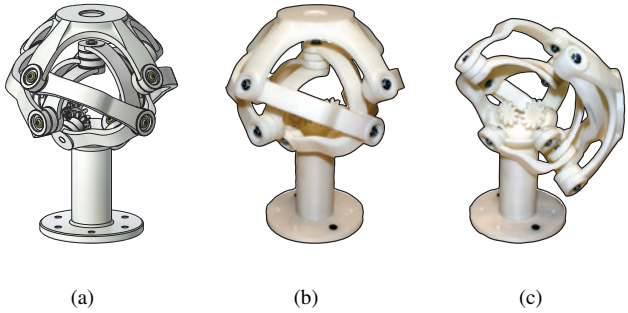

(a) (b) (c)

Fig. 12. A M_{2B}-ICPM with four $\mathfrak{m}_{2B}$-SCs (courtesy of Roberto Di Leva and Claudio Mazzotti). (a) CAD model of the wrist; (b) a prototype at initial configuration and (c) tilted configuration.

The proximal PM of the M_{2B}-ICPM, shown in Fig. 11(b), is a 2-DoF spherical PM, previously investigated in [61]. The M_{2B}-ICPM proposed here cannot be transformed into a M_{2B}-PM by removing the interconnecting revolute joints, because this would result in a $\mathrm{SO}(3)$-PM.

A novel 2-DoF wrist based on the M_{2B}-ICPM was presented in [60] and is shown in Fig. 12, which exhibits an extraordinary rotation (tilting) range of $\pm 90^\circ$ about any axis $\mathbf{w} = (\cos\phi, \sin\phi, 0)^{\mathrm{T}} \in \mathbb{R}^3, \phi \in [0, 2\pi)$, in comparison to $\pm 70^\circ$ of the 3-DoF parallel wrist "Agile Eye" [62] and $\pm 84^\circ$ of the 6-DoF general parallel manipulator reported in [10]. Another 2-DoF parallel wrist, the "Omni-wrist" [63], was reported to have the same rotation range as our M_{2B}-ICPM, but it lacks the advantage of having a fixed center of rotation. The readers may refer to [60] for more details about the analysis and design of this new wrist. □

***Example* 3** : M_{3A}-ICPM. Since M_{3A} is a parent SS of M_{2A}, its ICPM may be conveniently constructed based on that of M_{2A}. In order to generate an additional translational DoF along $\mathbf{e}_1 \in \mathfrak{m}_{3A}$, we may for example augment a $3\mathcal{R}$ $\mathfrak{m}_{2A}$-SC with another SP comprising two prismatic or helical joints. A practical alternative is to use a pair of parallelogram joints (denoted $\mathcal{P}_A$), resulting in the $\mathcal{R}\mathcal{P}_A\mathcal{R}\mathcal{P}_A\mathcal{R}$ $\mathfrak{m}_{3A}$-SCs as shown in Fig. 13. Note that according to the decomposition in Eq. (24), we have:

$$\underbrace{\{\mathbf{e}_1, \mathbf{e}_3, \mathbf{e}_4\}_{\text{span}}}_{\mathfrak{m}_{3A}} \oplus \underbrace{\{\mathbf{e}_2\}_{\text{span}}}_{\mathfrak{h}_{3A}} = \underbrace{\{\mathbf{e}_1, \mathbf{e}_2, \mathbf{e}_3, \mathbf{e}_4\}_{\text{span}}}_{\mathfrak{g}_{3A}} \tag{32}$$

The two $\mathcal{P}_A$ joints in the $\mathcal{P}_A$-SP should have equal projection onto the $\mathbf{xz}$-plane and equal and opposite projection along the $\mathbf{y}$-axis (see Fig. 13(b)).

We point out that although $\mathcal{P}_A$ is not a lower pair joint, its motion manifold may still be parameterized as the exponential image of a circular path $\boldsymbol{\xi}(\theta), \theta \in \mathbb{R}$ in $\{\mathbf{e}_1, \mathbf{e}_2, \mathbf{e}_3\}_{\text{span}}$. It is not difficult to verify that each of the $\mathcal{P}_A$-SPs as shown in Fig. 13 is instantaneously equivalent to a prismatic SP (as illustrated by the SP $(\boldsymbol{\xi}_1 + \boldsymbol{\eta}_1, \boldsymbol{\xi}_1 - \boldsymbol{\eta}_1)$ in Fig. 13(b)), and will be denoted by $(\boldsymbol{\xi}_{i2}^+, \boldsymbol{\xi}_{i2}^-), i = 1, ..., l$.

We may then proceed with *Step 2)* of Procedure 2:

$$\{\boldsymbol{\xi}_{i3}, \boldsymbol{\xi}_{i2}^-, \boldsymbol{\xi}_{i1}^-\}_{\text{span}} \oplus \mathfrak{h}_{3A} = \mathfrak{g}_{3A} \tag{33}$$

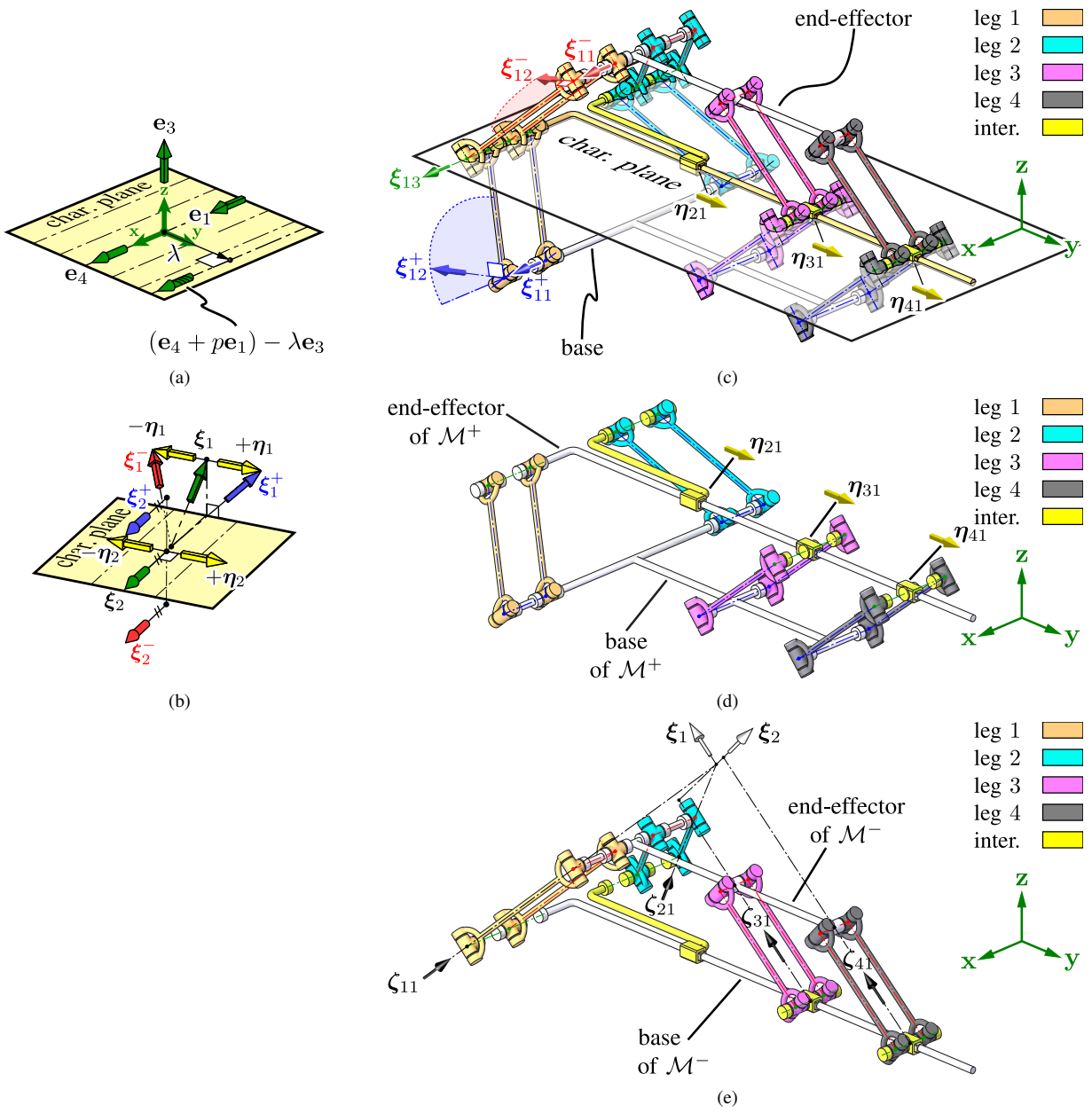

Fig. 13. Example of a M_{3A}-ICPM comprising four $\mathcal{RP}_A\mathcal{RP}_A\mathcal{R}$ $\mathfrak{m}_{3A}$-SCs. (a) screw system of $\mathfrak{m}_{3A}$; (b) various examples of $\mathfrak{m}_{3A}$-SPs; (c) joint twists of the ICPM (for clarity, only joint twists of leg 1 are shown); (d) proximal half PM; (e) distal half PM and constraint wrenches.

for all $i = 1, ..., l$. According to our construction, $(\boldsymbol{\xi}_{i3}, \boldsymbol{\xi}_{i1}^-) \oplus \{\mathbf{e}_2\}_{\text{span}} = \mathfrak{g}_{2A} = \{\mathbf{e}_2, \mathbf{e}_3, \mathbf{e}_4\}_{\text{span}}$ and therefore the $\mathcal{P}_A$-SP $(\boldsymbol{\xi}_{i2}^+, \boldsymbol{\xi}_{i2}^-)$ must have non-zero $\mathbf{e}_1$-components to satisfy Eq. (33).

Next, for *Step 3)* of Procedure 2, since $\mathfrak{h}_{3A} = \{\mathbf{e}_2\}_{\text{span}}$, each inter-SC chain should comprise one prismatic joint along the $\mathbf{y}$-axis at the initial configuration (yellow links and joints in Fig. 13).

Finally, for *Step 4)*, since $\mathfrak{g}_{3A}^\perp$ is a 2-system comprising all ∞-pitch wrenches perpendicular to the $\mathbf{x}$-axis and each distal half SC $\mathcal{M}_i^-$ contributes (after locking the proximal half PM) one additional constraint force, at least four SCs (rendered in light brown, cyan, pink and gray in Fig. 13) are needed to satisfy Eq. (26), i.e.,

$$\{\boldsymbol{\zeta}_{11}, ..., \boldsymbol{\zeta}_{41}\}_{\text{span}} \oplus \mathfrak{g}_{3A}^\perp = \mathfrak{se}(3)^* \tag{34}$$

or dually

$$\begin{aligned} &\{\boldsymbol{\zeta}_{11}^-, \boldsymbol{\zeta}_{21}^-, \boldsymbol{\zeta}_{31}^-, \boldsymbol{\zeta}_{41}^-\}_{\text{span}}^\perp \cap \mathfrak{g}_{3A} \\ &\quad = \{\boldsymbol{\xi}_1, \boldsymbol{\xi}_2\}_{\text{span}} \cap \{\mathbf{e}_1, \mathbf{e}_2, \mathbf{e}_3, \mathbf{e}_4\}_{\text{span}} = \mathbf{0} \end{aligned} \tag{35}$$

where $\boldsymbol{\xi}_1, \boldsymbol{\xi}_2$ are illustrated in Fig. 13(e). Equation (35) certainly holds, since the Shönflies algebra $\mathfrak{g}_{3A}$ contains no 0-pitch twists in the pencil spanned by $\boldsymbol{\xi}_1$ and $\boldsymbol{\xi}_2$.

As mentioned in Sec. I (see Fig. 4(a)), the M_{3A}-ICPM can tilt a line-symmetric object about the $\mathbf{x}$-axis, and also translate it in the $\mathbf{xy}$-plane. This, as we shall demonstrate in Sec. IV, serves as a potential candidate for an elbow exoskeleton.

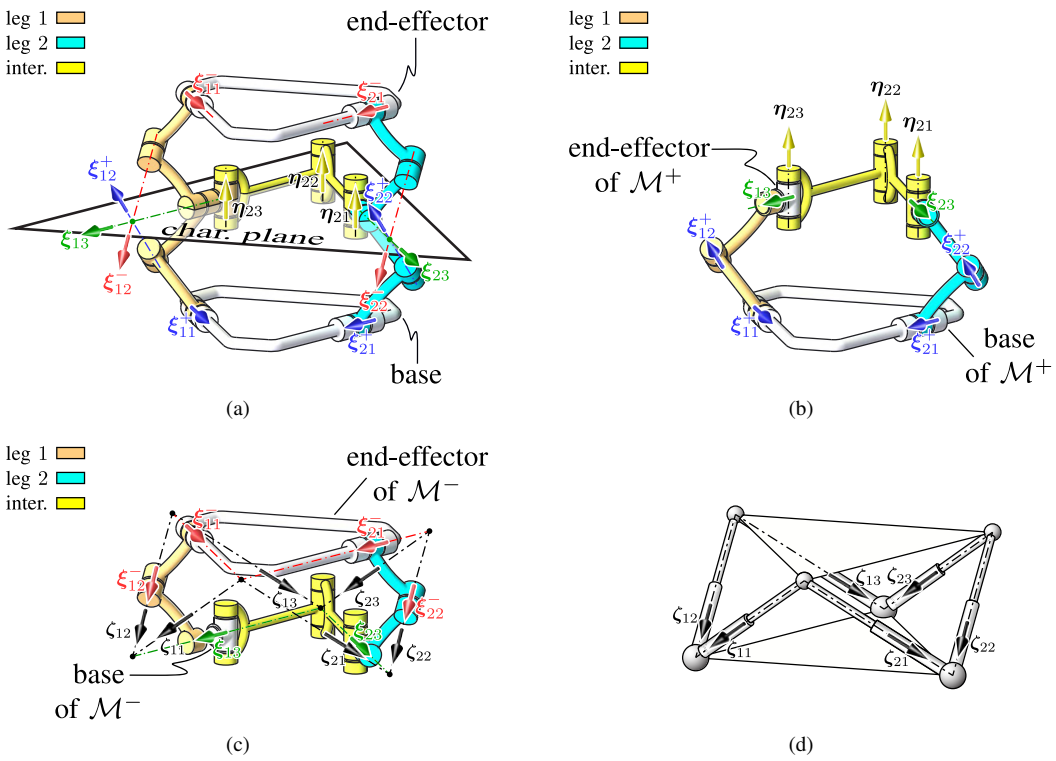

Fig. 14. Example of a M_{3B}-ICPM derived from the geometry of a 3-3 Gough-Stewart platform. It comprises two $5\mathcal{R}$ $\mathfrak{m}_{3B}$-SCs and one $\mathcal{RRR}$ inter-SC chain. (a) the M_{3B}-ICPM constructed based on Procedure 2; (b) the proximal half PM $\mathcal{M}^+$; (c) the distal half PM $\mathcal{M}^-$ and constraint wrenches; (d) equivalent geometry of a 3-3 Gough-Stewart platform (GSP).

We finally remark that the resulting $\mathfrak{m}_{3A}$-ICPM has an undeniably complex kinematic structure. We shall resolve this issue by introducing hybrid structure in Sec. III-B. □

***Example* 4** : M_{3B}-ICPM**.** Consider the synthesis of a M_{3B}-ICPM with l $5\mathcal{R}$ $\mathfrak{m}_{3B}$-SCs $\mathcal{M}_i = (\boldsymbol{\xi}_{i1}^+, \boldsymbol{\xi}_{i2}^+, \boldsymbol{\xi}_{i3}, \boldsymbol{\xi}_{i2}^-, \boldsymbol{\xi}_{i1}^-), i = 1, ..., l$. First, for *Step 2)* of Procedure 2, $\mathcal{M}_i^- = (\boldsymbol{\xi}_{i3}, \boldsymbol{\xi}_{i2}^-, \boldsymbol{\xi}_{i1}^-)$'s should satisfy:

$$\{\boldsymbol{\xi}_{i3}, \boldsymbol{\xi}_{i2}^-, \boldsymbol{\xi}_{i1}^-\}_{\text{span}} \oplus \underbrace{\{\mathbf{e}_1, \mathbf{e}_2, \mathbf{e}_6\}_{\text{span}}}_{\mathfrak{h}_{3B}} = \underbrace{\mathfrak{se}(3)}_{\mathfrak{g}_{3B}} \tag{36}$$

for all $i = 1, ..., l$. In other words, the screw system of $\{\boldsymbol{\xi}_{i3}, \boldsymbol{\xi}_{i2}^-, \boldsymbol{\xi}_{i1}^-\}_{\text{span}}$ should not intersect the planar algebra $\mathfrak{h}_{3B}$, i.e., it should not contain any 0-pitch screws parallel to the **z**-axis or any ∞-pitch screws perpendicular to the **z**-axis. Once $\mathcal{M}_i^-$ are determined, the $\mathfrak{m}_{3B}$-SCs $\mathcal{M}_i$ may simply be determined by mirror symmetry (see Fig. 5(b)).

Next, for *Step 3)*, since $\mathfrak{h}_{3B} = \{\mathbf{e}_1, \mathbf{e}_2, \mathbf{e}_6\}_{\text{span}}$ is a planar algebra, the inter-SC $\mathfrak{h}_{3B}$-chains are simply planar kinematic chains or even PMs, which can be synthesized using state-of-the-art methods [32]–[34].

Finally, for *Step 4)*, since each $\mathcal{M}_i^- = (\boldsymbol{\xi}_{i3}, \boldsymbol{\xi}_{i2}^-, \boldsymbol{\xi}_{i1}^-)$ contributes three linearly independent constraint wrenches $(\boldsymbol{\zeta}_{i1}, \boldsymbol{\zeta}_{i2}, \boldsymbol{\zeta}_{i3}), i = 1, ..., l$, at least two $\mathfrak{m}_{3B}$-SCs are needed to satisfy Eq. (26):

$$\begin{aligned}&(S_1^-)^\perp + (S_2^-)^\perp \\ &\quad = \{\boldsymbol{\zeta}_{11}, \boldsymbol{\zeta}_{12}, \boldsymbol{\zeta}_{13}, \boldsymbol{\zeta}_{21}, \boldsymbol{\zeta}_{22}, \boldsymbol{\zeta}_{23}\}_{\text{span}} = \mathfrak{se}(3)^*\end{aligned} \tag{37}$$

Note that since all joint twists of the $\mathfrak{m}_{3B}$-SCs are 0-pitch screws, $\boldsymbol{\xi}_{i3}, \boldsymbol{\xi}_{i2}^-, \boldsymbol{\xi}_{i1}^-$ should in general belong to one of the two reguli of a hyperboloid [57], while their (reciprocal) constraint wrenches $\boldsymbol{\zeta}_{i1}, \boldsymbol{\zeta}_{i2}, \boldsymbol{\zeta}_{i3}$ can be chosen as three 0-pitch wrenches lying on the other regulus of the hyperboloid. We end up with verifying the linear independence of six 0-pitch constraint wrenches, which is exactly the same as verifying the controllability (free of actuation singularity) of a Gough-Stewart platform [64]–[67], as illustrated in Fig. 14(d). We remark that the proposed M_{3B}-ICPM comprises one less $\mathfrak{m}_{3B}$-SC leg than the M_{3B}-PM shown in Fig. 5, and that the interconnecting $\mathfrak{h}_{3B}$-chain is responsible for providing an equivalent constraint of the missing leg.

As suggested in Sec. I (see Fig. 3(b), the proposed M_{3B}-ICPM can tilt a plane that initially coincides with the characteristic plane of $\mathfrak{m}_{3B}$ about any axis lying in the characteristic plane itself or translate it perpendicularly. We will discuss in Sec. IV its application in exoskeleton design. The proposed M_{3B}-ICPM may also serve as a novel 3-DoF CV coupling [39] due to its simplified structure.

□

***Example* 5** : M_4-ICPM**.** Consider the synthesis of a M_4-ICPM with l $\mathcal{UUUU}$ $\mathfrak{m}_4$-SCs:

$$\mathcal{M}_i = (\underbrace{\boldsymbol{\xi}_{i1}^+, \boldsymbol{\xi}_{i2}^+}_{\mathcal{U}}, \underbrace{\boldsymbol{\xi}_{i3}^+, \boldsymbol{\xi}_{i4}^+}_{\mathcal{U}}, \underbrace{\boldsymbol{\xi}_{i4}^-, \boldsymbol{\xi}_{i3}^-}_{\mathcal{U}}, \underbrace{\boldsymbol{\xi}_{i2}^-, \boldsymbol{\xi}_{i1}^-}_{\mathcal{U}}) \tag{38}$$

for $i = 1, ..., l$. In this case, S_i^- corresponds to a special four-system whose 0-pitch screws form a special congruence comprising two non-intersecting line pencils (see Fig. 15(c)) [57]. The reciprocal two-system $(S_i^-)^\perp$ is spanned by two

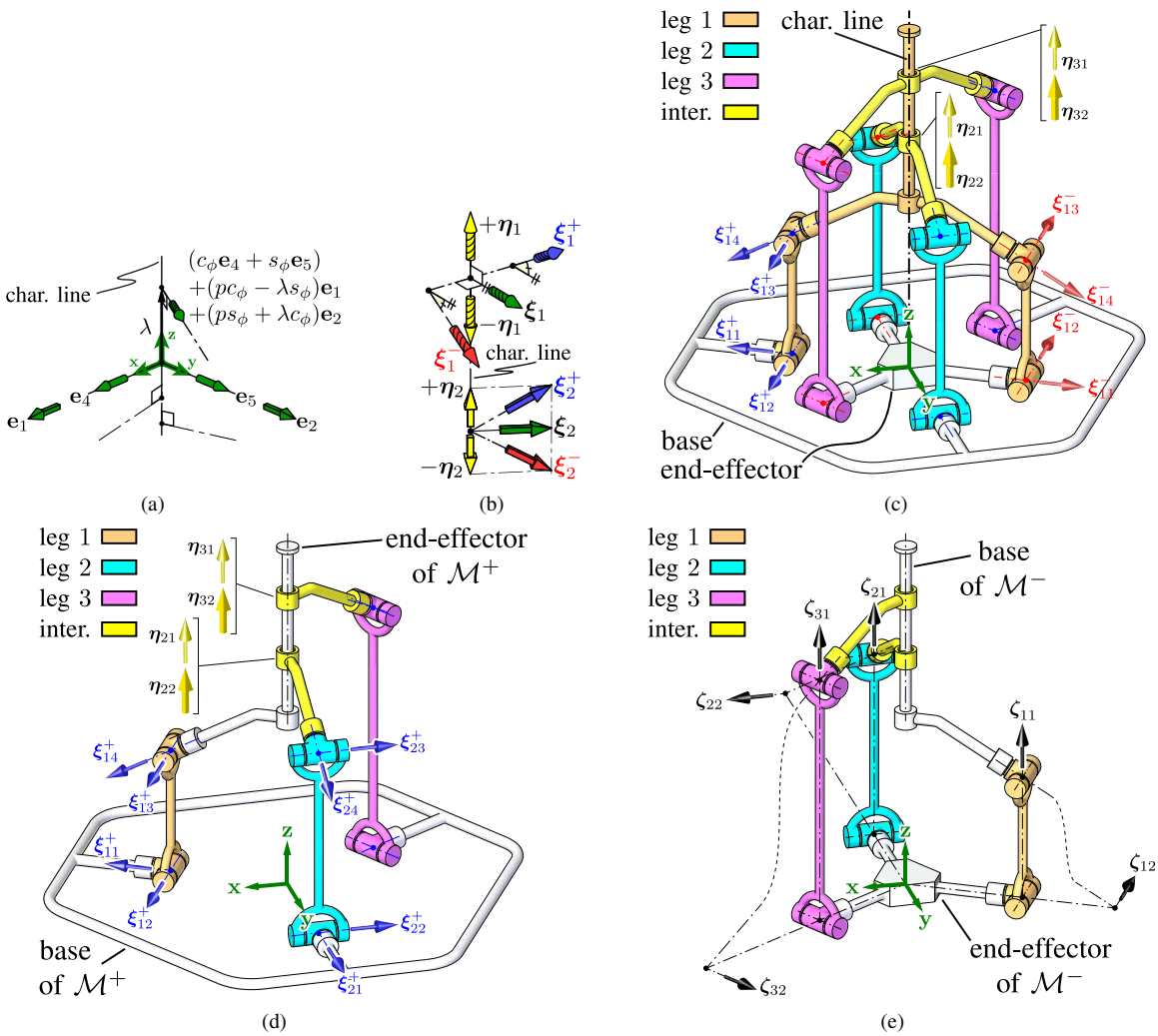

Fig. 15. Example of a M_4-ICPM. (a) Screw system of $\mathfrak{m}_4$; (b) various examples of $\mathfrak{m}_4$-SPs; (c) joint twists of the ICPM (for clarity, only joint twists of leg 1 are shown); (d) proximal half PM; (e) distal half PM and constraint wrenches (joint twists have been bent to generate a smaller figure).

conveniently identifiable 0-pitch wrenches $\boldsymbol{\zeta}_{i1}, \boldsymbol{\zeta}_{i2}$, namely along the line connecting the centers of the two line pencils and the line at the intersection of the pencil planes (see Fig. 15(e)).

For *Step 2)* of Procedure 2, $\mathcal{M}_i^- = (\boldsymbol{\xi}_{i4}^-, \boldsymbol{\xi}_{i3}^-, \boldsymbol{\xi}_{i2}^-, \boldsymbol{\xi}_{i1}^-)$ should satisfy:

$$\{\boldsymbol{\xi}_{i4}^-, \boldsymbol{\xi}_{i3}^-, \boldsymbol{\xi}_{i2}^-, \boldsymbol{\xi}_{i1}^-\}_{\text{span}} \oplus \underbrace{\{\mathbf{e}_3, \mathbf{e}_6\}_{\text{span}}}_{\mathfrak{h}_4} = \underbrace{\mathfrak{se}(3)}_{\mathfrak{g}_4} \tag{39}$$

or, dually

$$\underbrace{\{\boldsymbol{\zeta}_{i1}, \boldsymbol{\zeta}_{i2}\}_{\text{span}}}_{(S_i^-)^\perp} \cap \mathfrak{h}_4^\perp = \mathbf{0} \tag{40}$$

for all $i = 1, ..., l$. It can be shown using geometry of two-systems [57, Ch. 4] that this is equivalent to requiring $\boldsymbol{\zeta}_{i2}$ must not intersect the $\mathbf{z}$-axis. Once $\mathcal{M}_i^-$ is determined, the $\mathfrak{m}_4$-SC $\mathcal{M}_i$ may simply be determined by line symmetry (see Fig. 15(b)).

Next, for *Step 3)*, since $\mathfrak{h}_4 = \{\mathbf{e}_3, \mathbf{e}_6\}_{\text{span}}$ is the cylindrical algebra along the $\mathbf{z}$-axis, the inter-SC $\mathfrak{h}_4$-chains may simply be chosen as cylindrical joints, with joint twists denoted by $\boldsymbol{\zeta}_{i1}, \boldsymbol{\zeta}_{i2}$ for $i = 2, ..., l$ (yellow joints in Fig. 15).

Finally, for *Step 4)*, since each $\mathcal{M}_i^-$ each contributes two linearly independent constraint wrenches $(\boldsymbol{\zeta}_{i1}, \boldsymbol{\zeta}_{i2}), i = 1, ..., l$, at least three $\mathfrak{m}_4$-SCs are needed to satisfy Eq. (26):

$$\begin{aligned}(S_1^-)^\perp + (S_2^-)^\perp + (S_3^-)^\perp \\ = \{\boldsymbol{\zeta}_{11}, \boldsymbol{\zeta}_{12}, \boldsymbol{\zeta}_{21}, \boldsymbol{\zeta}_{22}, \boldsymbol{\zeta}_{31}, \boldsymbol{\zeta}_{32}\}_{\text{span}} = \mathfrak{se}(3)^*\end{aligned} \tag{41}$$

A possible choice is to arrange the six constraint wrenches in such a way that three ($\boldsymbol{\zeta}_{11}, \boldsymbol{\zeta}_{21}$ and $\boldsymbol{\zeta}_{31}$) span a parallel bundle of lines along the $\mathbf{z}$-axis whereas the remaining ($\boldsymbol{\zeta}_{12}, \boldsymbol{\zeta}_{22}$ and $\boldsymbol{\zeta}_{32}$) span a line field comprising 0-pitch screws in the $\mathbf{xy}$-plane (see Fig. 15(e)).

As suggested in Sec. I (see Fig. 4(b)), the proposed M_4-ICPM serves as a line-symmetric motion generator and consequently has numerous related applications. First, since the end-effector of the ICPM may tilt about any point on the $\mathbf{z}$-axis and may also translate in the $\mathbf{xy}$-plane, it may serve as a remote center of motion (RCM) mechanism for use in minimum invasive surgery. Along with an additional prismatic axis (see Sec. III-B), it may also serve as a five-axis machine,

a haptic interface or a 5-DoF passive axis-alignment device for 1-DoF human elbow exoskeleton device (see our discussion in Sec. IV). □

We have so far illustrated the universality and effectiveness of generating SS motion manifolds with ICPMs following Procedure 2. We emphasize that the reported examples have been chosen to involve only a few special screw systems, which suffice to illustrate the core idea of Procedure 2. A full spectrum of synthesis results based on the geometry of more general screw systems may be performed and it will be reported in our future work.

B. Synthesis of serial-parallel hybrid manipulators

Although none of the seven SSs admits POE representations, it turns out that two SSs, namely M_5 and M_{3A}, may in fact be decomposed into the product of exponentials of two complementary subspaces of their LTSs, i.e.

$$\exp\mathfrak{m} = \exp\mathfrak{u}\cdot\exp\mathfrak{v} \qquad \mathfrak{u}\oplus\mathfrak{v} = \mathfrak{m} \tag{42}$$

in a neighborhood of $\mathbf{I}$. We refer to $(\mathfrak{u},\mathfrak{v})$ as an *exponential pair* of $\mathfrak{m}$.

***Theorem* 2.** Up to conjugation, the only exponential pairs $(\mathfrak{u},\mathfrak{v})$ for LTSs of $\mathfrak{se}(3)$ are the following:

1) $\mathfrak{m}_{3A} = \{\mathbf{e}_1,\mathbf{e}_3,\mathbf{e}_4\}_{\text{span}}$ admits an exponential pair $(\mathfrak{u},\mathfrak{v})$ such that $\mathfrak{u} = \{\mathbf{e}_1\}_{\text{span}}$ and $\mathfrak{v}$ is any complementary subspace of $\mathfrak{u}$ in $\mathfrak{m}_{3A}$.
2) $\mathfrak{m}_5 = \{\mathbf{e}_1,\mathbf{e}_2,\mathbf{e}_3,\mathbf{e}_4,\mathbf{e}_5\}_{\text{span}}$ admits the following exponential pairs $(\mathfrak{u},\mathfrak{v})$:
   (a) $\mathfrak{u} = \{\mathbf{e}_3 + p\mathbf{e}_1\}_{\text{span}}$
   (b) $\mathfrak{u} = \{\mathbf{e}_3\}_{\text{span}}$
   (c) $\mathfrak{u} = \{\mathbf{e}_1,\mathbf{e}_2 + p\mathbf{e}_3\}_{\text{span}}$
   (d) $\mathfrak{u} = \{\mathbf{e}_1,\mathbf{e}_3\}_{\text{span}}$
   (e) $\mathfrak{u} = \{\mathbf{e}_1,\mathbf{e}_2,\mathbf{e}_3\}_{\text{span}}$

   For each case above, $\mathfrak{v}$ is any complementary subspace of $\mathfrak{u}$ in $\mathfrak{m}_5$. □

The proof of the above theorem is beyond the scope of this paper and will be reported in a separate paper [68]. However one may easily verify the above claims by direct computation. Notice that the choice of the complementary subspace $\mathfrak{v}$ is limited by the fact that $\mathfrak{u}$ is always a Lie subalgebra. Therefore, $\mathfrak{v}$ cannot be a Lie subalgebra for otherwise $\exp\mathfrak{m}$ would admit a POE representation. Moreover, the subspace $\mathfrak{v}$ must be properly chosen so that the corresponding exponential submanifold $\exp\mathfrak{v}$ is synthesizable: this implies that, within the framework of this paper, $\mathfrak{v}$ must be a LTS. A straightforward verification using all possible LTSs leads to an exhaustive list of exponential pairs $(\mathfrak{u},\mathfrak{v})$ as shown in Tab. I.

It follows from Theorem 2 that the concatenation of a $\exp\mathfrak{u}$-generator and a $\exp\mathfrak{v}$-generator is a generator of $\exp\mathfrak{m} = \exp\mathfrak{u}\cdot\exp\mathfrak{v}$, resulting in what we call a serial-parallel hybrid manipulator (SPHM). Since $\mathfrak{u}$ is always a Lie subalgebra of $\mathfrak{se}(3)$, $\exp\mathfrak{u}$ may be realized by either a serial chain or a PM, which can be synthesized using state-of-the-art type synthesis methods [32]–[36]. On the other hand, all $\mathfrak{v}$'s appear to be LTSs of dimension 2 to 4, and therefore they may be generated either by PMs (Sec. II-B) or by ICPMs (Sec. III-A). The same motion manifolds may also be generated by a pair of cooperating motion modules generating $\exp\mathfrak{u}$ and $\exp\mathfrak{v}$ respectively [45]. We also emphasize that Theorem 2 enables us to synthesize motion generators for M_5 where Procedure 2 is not applicable. We can also avoid directly synthesizing a M_{3A}-ICPM (resulting in a complex kinematic structure) by concatenating a M_{2A}-ICPM with a prismatic joint. We shall see some of these examples in Sec. IV.

TABLE I
SYNTHESIZABLE EXPONENTIAL PAIRS OF LTSS OF $\mathfrak{se}(3)$

$\mathfrak{m}$	$\mathfrak{u}$	$\mathfrak{v}$
$\mathfrak{m}_{3A}$	$\{\mathbf{e}_1\}_{\text{span}}$	$\{\mathbf{e}_3+p\mathbf{e}_1,\mathbf{e}_4\}_{\text{span}} = \mathfrak{m}_{2A}^{(p)}$
$\mathfrak{m}_5$	$\{\mathbf{e}_1+p\mathbf{e}_3\}_{\text{span}}, p\neq 0$	$\{\mathbf{e}_1,\mathbf{e}_2,\mathbf{e}_4,\mathbf{e}_5\}_{\text{span}} = \mathfrak{m}_4$
	$\{\mathbf{e}_3\}_{\text{span}}$	$\{\mathbf{e}_1,\mathbf{e}_2,\mathbf{e}_4,\mathbf{e}_5\}_{\text{span}} = \mathfrak{m}_4$
	$\{\mathbf{e}_1,\mathbf{e}_2+p\mathbf{e}_3\}_{\text{span}}$	$\{\mathbf{e}_3,\mathbf{e}_4,\mathbf{e}_5\}_{\text{span}} = \mathfrak{m}_{3B}$
	$\{\mathbf{e}_1,\mathbf{e}_3\}_{\text{span}}$	no LTS available
	$\{\mathbf{e}_1,\mathbf{e}_2,\mathbf{e}_3\}_{\text{span}}$	$\{\mathbf{e}_4,\mathbf{e}_5\}_{\text{span}} = \mathfrak{m}_{2B}$

To summarize, we have so far established an overarching framework for type synthesis of symmetric subspace motion generators, which includes:

(i) synthesis of PMs for M_{2A},M_{2B} and M_{3B};
(ii) synthesis of ICPMs for $\mathrm{M}_{2A}^{(p)}$,M_{2B},M_{3A},M_{3B} and M_4;
(iii) synthesis of SPHMs for M_{3A} and M_5.

IV. APPLICATION OF SYMMETRIC SUBSPACE MOTION GENERATORS

As pointed out in Sec. I, the symmetric subspaces of $\mathrm{SE}(3)$ may serve as motion manifolds for the manipulation of objects with revolute, line and plane symmetry. Such manipulation tasks have a broad range of applications in robotics, but have not been systematically investigated before. This section applies the SS-motion generators synthesized in the previous sections to some key applications involving manipulating objects with symmetry.

A. Revolute Symmetry in Five-Axis Machining and Haptic Interfaces

It is pointed out in Sec. I that the 2D SS M_{2B} captures the geometry of orientating an object with revolute symmetry over the unit 2-sphere S^2. It follows that the 5D SS M_5 is exactly the motion manifold characterizing the displacement of revolute-symmetric objects in the sense of Theorem 2:

$$\mathrm{M}_5 = \mathrm{T}_3\cdot\mathrm{M}_{2B} \tag{43}$$

where T_3 denotes the 3D translational subgroup $\exp\{\mathbf{e}_1,\mathbf{e}_2,\mathbf{e}_3\}_{\text{span}}$. Immediate applications include five-axis machining [45] and haptic interfaces [69], where the self-spin of the spindle/stylus is not essential. One may argue that, in this case, the 2D POE $\exp\{\mathbf{e}_4\}_{\text{span}}\cdot\exp\{\mathbf{e}_5\}_{\text{span}}$ (generating the motion of a Cardan joint) may well be used in place of M_{2B}. However, the Cardan model suffers from parametrization singularity at 90° tilt [70]. In comparison, $\mathrm{M}_{2B} = \exp\{\mathbf{e}_4,\mathbf{e}_5\}_{\text{span}}$ enjoys an almost (except at 180° tilt) singularity-free orientation

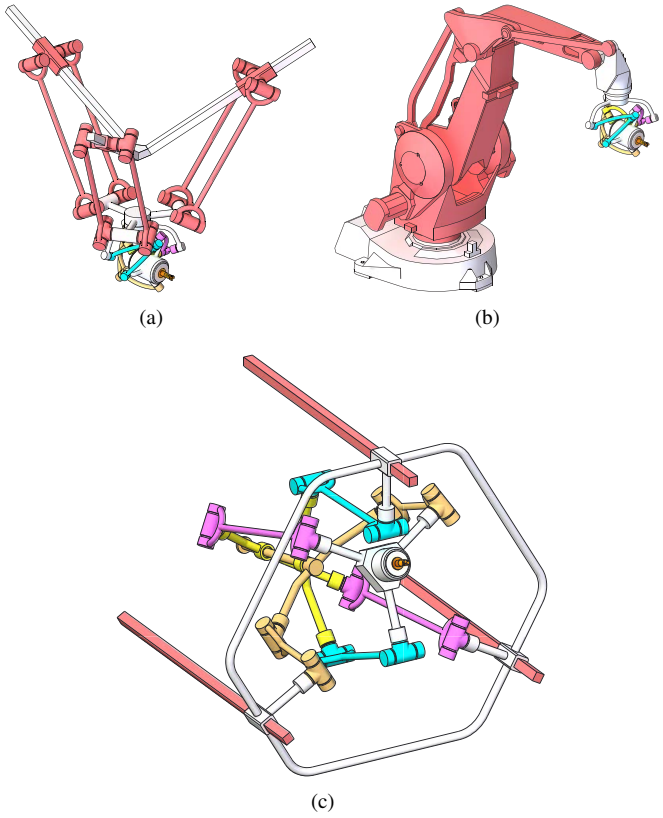

Fig. 16. (a) A M_5-SPHM comprising a PM translational module (a linear DELTA robot in red) and a M_{2B}-ICPM module; (b) a M_5-SPHM comprising a serial translational module (an ABB IRB260 robot in red) and a M_{2B}-ICPM module; (c) a M_5-SPHM comprising a $\mathcal{P}$ joint (in red) and a M_4-ICPM module.

parametrization [60], and does lead to PM (ICPM) designs with omni-directional 90° tilt range [71,72].

Referring to Eq. (43), we may design a five-axis SPHM comprising a T_3-module concatenated with the M_{2B}-ICPM (shown in Fig. 11(a)). For example, we may realize the T_3-module by a PM (as shown by the red linear DELTA in Fig. 16(a)) or also a serial robot [73] (as shown in Fig. 16(b) by the red ABB IRB260 palletizer). Note that although the latter also produces a involuntary rotation about the $\mathbf{z}$-axis, the SPHM is nevertheless legitimate since M_{2B} is invariant under such a rotation (with its isotropy group being $\mathrm{H}_{2B} = \mathrm{SO}(2)$).

If, on the other hand, the traveling range in one direction, say along the $\mathbf{z}$-axis, is required to be larger than the other freedoms, we may use a different decomposition of M_5, such as:

$$\mathrm{M}_5 = \mathrm{T}_{\mathbf{z}} \cdot \mathrm{M}_4 \tag{44}$$

where $\mathrm{T}_{\mathbf{z}}$ denotes $\exp\{\mathbf{e}_3\}_{\mathrm{span}}$, leading to a M_5-SPHM with a M_4-ICPM module mounted on a linear rail, as shown in Fig. 16(c).

B. Line symmetry in Needle Positioning for Minimal Invasive Surgery

M_4, historically known as the space of line symmetric motions [21,74], characterizes the motion manifold of a line-symmetric object by screwing it along the common perpendicular of its symmetry axis at the initial and final locations (see

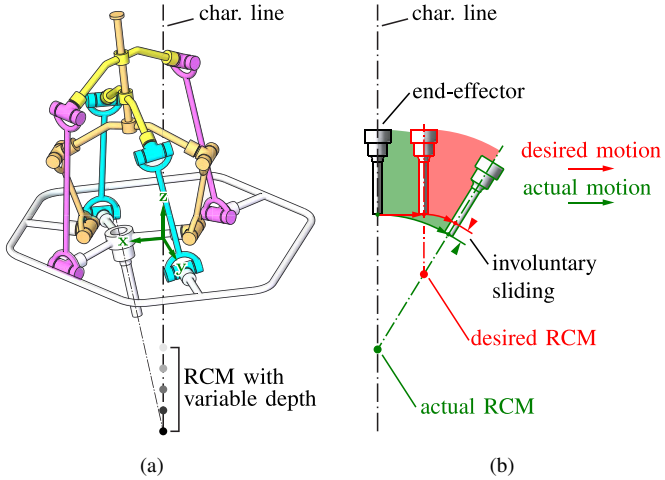

Fig. 17. Application of M_4-ICPM in needle positioning for minimal invasive surgery. (a) Any point on the characteristic line is a RCM for the end-effector; (b) a point not on the characteristic line may serve as a pseudo RCM (i.e., with involuntary sliding).

Fig. 4). Although line symmetric motions in general do not correspond to shortest paths under any physically meaningful Riemannian metric on $\mathrm{SE}(3)$ [75], they avoid introducing undesired spin motion about the symmetry axis, a property that is desired in needle positioning for minimal invasive surgery [26,76].

State-of-the-art designs of minimal invasive surgery robot either implement a 3R1T POE ($\exp\{\mathbf{e}_4\}_{\mathrm{span}} \cdot \exp\{\mathbf{e}_5\}_{\mathrm{span}} \cdot \exp\{\mathbf{e}_6\}_{\mathrm{span}} \cdot \exp\{\mathbf{e}_3\}_{\mathrm{span}}$) motion generator with combined needle positioning and insertion functionality [77,78], or a 2T2R POE ($\exp\{\mathbf{e}_1\}_{\mathrm{span}} \cdot \exp\{\mathbf{e}_2\}_{\mathrm{span}} \cdot \exp\{\mathbf{e}_4\}_{\mathrm{span}} \cdot \exp\{\mathbf{e}_5\}_{\mathrm{span}}$) motion generator for needle positioning (equipped with an additional axis for needle insertion) [79]. The RCM of the robot is fixed to a single point in the former case, and is allowed to translate in the $\mathbf{xy}$-plane in the latter case. The problems with such designs are: i) additional depth alignment is needed to match the needle insertion point with the RCM or RCM plane; ii) the line symmetry of the needle positioning task is not identified in either case, resulting in RCM mechanism designs that introduce involuntary spin of the needle.

On the other hand, since the M_4-ICPM proposed in Fig. 15 can rotate its end-effector about any axis that perpendicularly intersects the characteristic line of $\mathfrak{m}_4$ (Fig. 15(a)), any point on the characteristic line is one of its RCMs (as illustrated in Fig. 17(a)). This allows the M_4-ICPM to accomplish the needle positioning task free of involuntary spin, and also being able to accommodate uncertain insertion point depth. If the desired insertion point does not lie on the characteristic line (as shown by the red RCM in Fig. 17(b)), it is still possible to move the end-effector as if it first translates above and rotates about the desired RCM and then undergoes an involuntary sliding along the symmetry axis of the end-effector (as shown in Fig. 17(b)). Consequently, the "pseudo" RCM (in red) may still serve as the needle insertion point if the needle is initially not in contact with the patient.

C. Plane Symmetry in Axis-Misalignment Tolerant Design of Exoskeletons

Aside from characterizing the motion of the modules of a hyper-redundant robot, plane-symmetric motions may also have following potential application. In biomechanics, human joints such as 1-DoF elbow/knee joint or 3-DoF shoulder joint are rarely modeled as revolute or spherical joints due to the presence of joint axis sliding motion [80]. For example, an accurate kinematic model of the human knee joint is proposed by Parenti-Castelli *et al.* [81,82], which leads to an equivalent 5-$\mathcal{SS}$ PM model. Such model is important for understanding and simulating the biomechanics of human joint, but is rarely considered in ergonomic design of wearable exoskeleton due to its complexity.

An alternative approach is to model the human joints as revolute or spherical joints, and provide additional freedoms to accommodate the inevitable axis misalignment between the human joint axis and the exoskeleton joint axis [27]–[31]. By assuming the elbow joint to be a planar joint, Stienen *et al.* [28] proposed to use a 2T $\mathcal{P}_A\mathcal{P}_A$ passive mechanism to accommodate planar axis misalignment of an elbow exoskeleton joint to the human counterpart, as illustrated in Fig. 18(a). Such design corresponds, up to conjugation, to the following decomposition of the planar Euclidean group $\mathrm{SE}(2) = \exp\{\mathbf{e}_2, \mathbf{e}_3, \mathbf{e}_4\}_{\mathrm{span}}$:

$$\mathrm{SE}(2) = \exp\{\mathbf{e}_4\}_{\mathrm{span}} \cdot \exp\{\mathbf{e}_2, \mathbf{e}_3\}_{\mathrm{span}} \tag{45}$$

Note that both translational DoFs are needed for generating a finite rotation about the misaligned human elbow joint. On the other hand, we may also model the elbow exoskeleton after the GPD for $\mathrm{G}_{2A} = \mathrm{SE}(2)$:

$$\mathrm{SE}(2) = \mathrm{M}_{2A} \cdot \exp\{\mathbf{e}_2\}_{\mathrm{span}} \tag{46}$$

leading to an active M_{2A}-ICPM elbow exoskeletal joint with a passive $\mathcal{P}$ joint for axis misalignment, as shown in Fig. 18(c),(d). The M_{2A}-ICPM comprises one $\mathcal{RPPR}$ and two $\mathcal{RRR}$ $\mathfrak{m}_{2A}$-SCs, and exhibits a much larger rotation range in comparison to the M_{2A}-ICPM illustrated in Fig. 10(a) to match the motion range of the human elbow joint. A differential mechanism may be employed to drive the active joint by one input. Note that in this case, axis alignment is achieved so long as the human elbow axis is aligned with the characteristic plane of the M_{2A}-ICPM. Such design therefore leads to a reduced motion range of the alignment mechanism. If elbow laxity [31] is taken into consideration, we may simply replace the GPD of G_{2A} with that of $\mathrm{G}_{3A} = \exp\{\mathbf{e}_1, \mathbf{e}_2, \mathbf{e}_3, \mathbf{e}_4\}_{\mathrm{span}}$:

$$\mathrm{G}_{3A} = \mathrm{M}_{3A} \cdot \exp\{\mathbf{e}_2\}_{\mathrm{span}} = \mathrm{M}_{2A} \cdot \exp\{\mathbf{e}_1, \mathbf{e}_2\}_{\mathrm{span}} \tag{47}$$

where the second equality is due to Theorem 2. This leads to an elbow exoskeleton design with an active M_{2A} joint and a 2T passive alignment mechanism.

A 3D version of the exoskeleton we have designed can be similarly developed for the 3-DoF shoulder joint by resorting to the GPD of M_{3B}:

$$\mathrm{SE}(3) = \mathrm{M}_{3B} \cdot \mathrm{SE}(2) \tag{48}$$

Our analysis also suggests that the design of such exoskeletons is closely related to the plane symmetric motions of M_{2A} and M_{3B} (as illustrated in Fig. 3), since their corresponding motion generators can efficiently accommodate axis misalignment by providing a parallel pencil and a planar field of rotation axes respectively. Finally, the GPD of $\mathrm{G}_4 = \mathrm{SE}(3)$ can be exploited in the design of elbow exoskeletons if a more sophisticated elbow joint model [31] is considered.

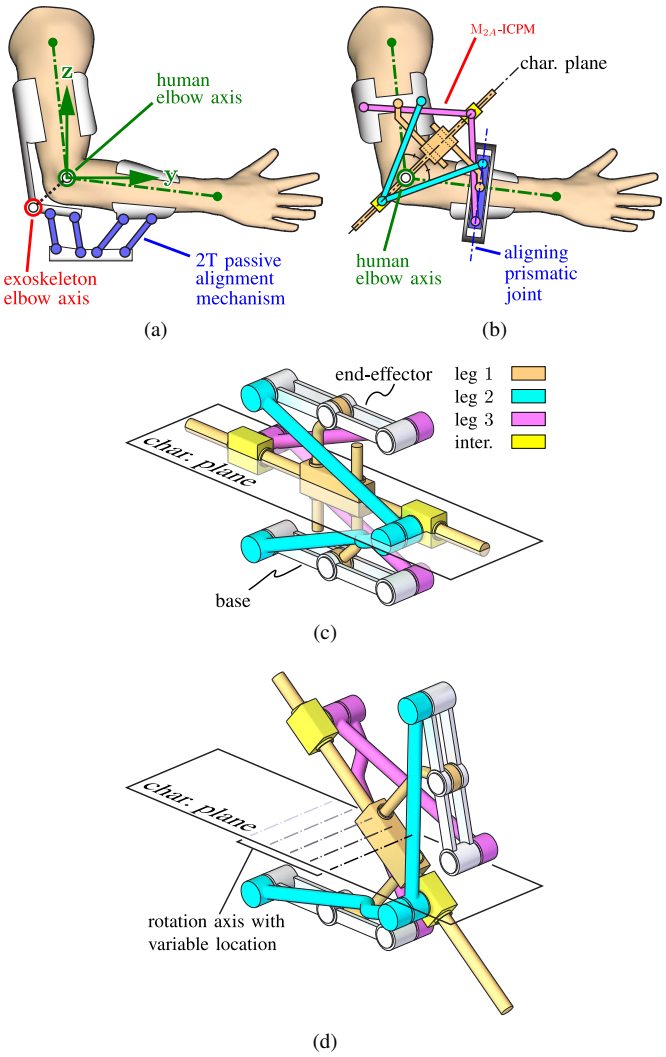

Fig. 18. Elbow exoskeleton with axis alignment mechanisms. (a) $\mathcal{R}$-type elbow joint with 2T $\mathcal{P}_A\mathcal{P}_A$ alignment mechanism; (b) M_{2A}-type joint with 1T $\mathcal{P}$ alignment mechanism; (c) proposed M_{2A}-ICPM design; (d) variable location of rotation axis of the M_{2A}-ICPM.

V. Conclusion

In this paper, we presented an overarching type synthesis framework of symmetric subspace motion generators for functionally redundant manipulation of 3D shapes with continuous symmetry. We demonstrated the effectiveness of our synthesis procedure by presenting, for each symmetric subspace, one or two novel motion generators, and demonstrated their potential applications. In order to focus on developing the core ideas, we refrain from presenting exhaustive enumeration of synthesis results.

Our work has demonstrated, using practical robotic applications, the existence of motion manifolds outside the product-

of-exponentials category and the necessity and means of addressing their type synthesis problem. On the one hand, we have provided ample opportunities for further research on type synthesis and conceptual design of parallel robots with inherently superior kinematic/dynamic performance (for functionally redundant manipulation tasks). On the other hand, the geometric properties of the symmetric subspaces demonstrated via their type synthesis may also be beneficial to planning, estimation and control of robotic systems having either their motion manifolds or their kinematic structures exhibiting certain types of symmetry.

ACKNOWLEDGMENT

We would like to thank Prof. Harald Löwe for his help with Theorem 2. The first author would also like to acknowledge the China National Natural Science Foundation Grant No. 51375413 for partially supporting him when he was working in HKUST.

APPENDIX A
ELEMENTS OF THE SPECIAL EUCLIDEAN GROUP SE(3)

The following notations are used throughout this paper, and are reasonably consistent with those in [13,33,83]. As we shall not give any introduction to Lie group theory of $\mathrm{SE}(3)$ or the screw geometry of $\mathfrak{se}(3)$, the readers should refer to authoritative texts for further details [57,83,84]. We only remark that the former are mainly used in the proofs of the theorems and synthesis procedures presented in this paper, and the latter is extensively used in presenting the synthesis results.

Elements of $\mathrm{SE}(3)$, denoted $\mathbf{g}, \mathbf{h}, ...$, are understood to be homogeneous matrices of the form:

$$\mathbf{g} = \begin{pmatrix} \mathbf{R} & \mathbf{t} \\ \mathbf{0}^T & 1 \end{pmatrix} \in \mathbb{R}^{4\times 4} \tag{A.1}$$

with $\mathbf{R}$ a proper orthogonal matrix, i.e. $\mathbf{R} \in \mathrm{SO}(3)$, and $\mathbf{t}$ an arbitrary vector in $\mathbb{R}^3$ representing the rotation and translation component respectively.

Elements of the Lie algebra $\mathfrak{se}(3)$ of $\mathrm{SE}(3)$ are often referred to as *twists*, and are denoted by $\boldsymbol{\xi}, \boldsymbol{\eta}, ...$ (c.f. $\widehat{\boldsymbol{\xi}}$ in [83]):

$$\boldsymbol{\xi} = \begin{pmatrix} \widehat{\mathbf{w}} & \mathbf{v} \\ \mathbf{0}^T & 0 \end{pmatrix} \in \mathbb{R}^{4\times 4} \tag{A.2}$$

where $\mathbf{w}, \mathbf{v} \in \mathbb{R}^3$ and $\widehat{\mathbf{w}}$ denotes the 3×3 skew-symmetric matrix corresponding to $\mathbf{w}$ such that $\widehat{\mathbf{w}}\mathbf{w}' = \mathbf{w} \times \mathbf{w}'$, $\forall \mathbf{w}' \in \mathbb{R}^3$. The exponential map $\exp : \mathfrak{se}(3) \to \mathrm{SE}(3)$ is defined by:

$$\exp \boldsymbol{\xi} = \mathbf{I} + \boldsymbol{\xi} + \frac{1}{2!}\boldsymbol{\xi}^2 + \frac{1}{3!}\boldsymbol{\xi}^3 + \cdots \qquad \forall \boldsymbol{\xi} \in \mathfrak{se}(3) \tag{A.3}$$

With an abuse of notation, we also use $\boldsymbol{\xi}, \boldsymbol{\eta}, ...$ to denote the *axis-coordinates* [84] of Eq. (A.2):

$$\boldsymbol{\xi} = \begin{pmatrix} \mathbf{v} \\ \mathbf{w} \end{pmatrix} \in \mathbb{R}^6 \tag{A.4}$$

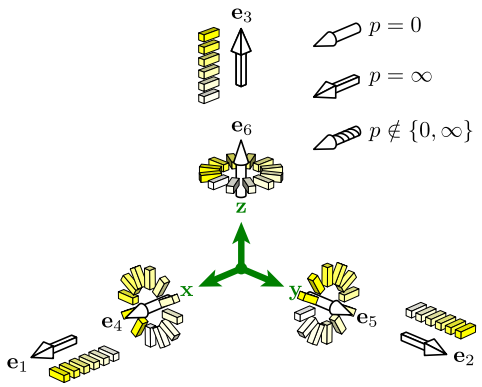

Fig. A.1. Graphical representation of the canonical basis of $\mathfrak{se}(3)$ and notation for twists with different pitch value p.

with $\mathbf{w}$ and $\mathbf{v}$ representing the angular and linear velocity respectively. Consequently, the canonical basis of $\mathbb{R}^6$, denoted $\mathbf{e}_1, ..., \mathbf{e}_6$,

$$\begin{aligned} \mathbf{e}_1 &= \begin{pmatrix} \mathbf{x} \\ \mathbf{0} \end{pmatrix} & \mathbf{e}_2 &= \begin{pmatrix} \mathbf{y} \\ \mathbf{0} \end{pmatrix} & \mathbf{e}_3 &= \begin{pmatrix} \mathbf{z} \\ \mathbf{0} \end{pmatrix} \\ \mathbf{e}_4 &= \begin{pmatrix} \mathbf{0} \\ \mathbf{x} \end{pmatrix} & \mathbf{e}_5 &= \begin{pmatrix} \mathbf{0} \\ \mathbf{y} \end{pmatrix} & \mathbf{e}_6 &= \begin{pmatrix} \mathbf{0} \\ \mathbf{z} \end{pmatrix} \\ \mathbf{x} &= (1,0,0)^T & \mathbf{y} &= (0,1,0)^T & \mathbf{z} &= (0,0,1)^T \end{aligned} \tag{A.5}$$

also define a set of basis twists for $\mathfrak{se}(3)$, with $\mathbf{e}_1, \mathbf{e}_2, \mathbf{e}_3$ (respectively, $\mathbf{e}_4, \mathbf{e}_5, \mathbf{e}_6$) representing unit instantaneous translation (respectively, rotation) along the $\mathbf{x}, \mathbf{y}, \mathbf{z}$ axes respectively (see Fig. A.1).

Elements of $\mathfrak{se}(3)^*$, the dual space of $\mathfrak{se}(3)$, are referred to as *wrenches* and denoted, in ray coordinates, by $\boldsymbol{\zeta}$:

$$\boldsymbol{\zeta} = \begin{pmatrix} \mathbf{f} \\ \boldsymbol{\tau} \end{pmatrix} \tag{A.6}$$

with $\mathbf{f}$ (force component) and $\boldsymbol{\tau}$ (torque component) pairing with $\mathbf{v}$ and $\mathbf{w}$ respectively. In this case, the natural pairing $\langle \cdot, \cdot \rangle$ between $\mathfrak{se}(3)^*$ and $\mathfrak{se}(3)$ is simply given by the inner product:

$$\langle \boldsymbol{\zeta}, \boldsymbol{\xi} \rangle := \boldsymbol{\zeta}^T \cdot \boldsymbol{\xi} \tag{A.7}$$

APPENDIX B
SYMMETRIC SUBSPACES OF SE(3) AND THEIR SYMMETRIC TWIST PAIRS

A symmetric subspace M of $\mathrm{SE}(3)$, like a Lie subgroup of $\mathrm{SE}(3)$, is uniquely determined by its identity tangent space $\mathfrak{m} := \mathrm{T}_{\mathbf{I}}\mathrm{M}$, which is closed under double commutators

$$[[\boldsymbol{\xi}_1, \boldsymbol{\xi}_2], \boldsymbol{\xi}_3] \in \mathfrak{m} \quad \forall \boldsymbol{\xi}_1, \boldsymbol{\xi}_2, \boldsymbol{\xi}_3 \in \mathfrak{m} \tag{B.1}$$

and hence is referred to as a *Lie triple subsystem* (LTS) [14]. More precisely, M is the exponential image of $\mathfrak{m}$[4]

$$\mathrm{M} = \exp \mathfrak{m} \tag{B.2}$$

A total of seven conjugacy classes of symmetric subspaces of $\mathrm{SE}(3)$ have been found in [13], and recalled here in

[4]An exception is $\mathfrak{m}^p_{2A}, p \neq 0$, where M^p_{2A} is generated from $\exp \mathfrak{m}^p_{2A}$ by inversion symmetry [13].

TABLE B.1
CONJUGACY CLASSES OF SS'S OF SE(3) (EXCLUDING LIE SUBGROUPS OF SE(3), WHICH ARE TRIVIAL SS'S).

dim	M	$\mathfrak{m}$ (normal form)	$\mathfrak{h}_\mathfrak{m}=[\mathfrak{m},\mathfrak{m}]$	$\mathfrak{g}_\mathfrak{m}=\mathfrak{h}_\mathfrak{m}+\mathfrak{m}$	isotropy group
2	$\mathrm{M}_{2A}^{(p)}$	$\mathfrak{m}_{2\mathrm{A}}^{(p)}\triangleq\{\mathbf{e}_3,\mathbf{e}_4+p\mathbf{e}_1\}_{\mathrm{span}}$	$\{\mathbf{e}_2\}_{\mathrm{span}}$	$\{\mathbf{e}_2,\mathbf{e}_3,\mathbf{e}_4+p\mathbf{e}_1\}_{\mathrm{span}}$	$\exp\{\mathbf{e}_1,\mathbf{e}_2\}_{\mathrm{span}}$
	M_{2B}	$\mathfrak{m}_{2\mathrm{B}}\triangleq\{\mathbf{e}_4,\mathbf{e}_5\}_{\mathrm{span}}$	$\{\mathbf{e}_6\}_{\mathrm{span}}$	$\{\mathbf{e}_4,\mathbf{e}_5,\mathbf{e}_6\}_{\mathrm{span}}$	$\exp\{\mathbf{e}_6\}_{\mathrm{span}}$
3	M_{3A}	$\mathfrak{m}_{3\mathrm{A}}\triangleq\{\mathbf{e}_1,\mathbf{e}_3,\mathbf{e}_4\}_{\mathrm{span}}$	$\{\mathbf{e}_2\}_{\mathrm{span}}$	$\{\mathbf{e}_1,\mathbf{e}_2,\mathbf{e}_3,\mathbf{e}_4\}_{\mathrm{span}}$	$\exp\{\mathbf{e}_1,\mathbf{e}_2\}_{\mathrm{span}}$
	M_{3B}	$\mathfrak{m}_{3\mathrm{B}}\triangleq\{\mathbf{e}_3,\mathbf{e}_4,\mathbf{e}_5\}_{\mathrm{span}}$	$\{\mathbf{e}_1,\mathbf{e}_2,\mathbf{e}_6\}_{\mathrm{span}}$	$\mathfrak{se}(3)$	$\exp\{\mathbf{e}_1,\mathbf{e}_2,\mathbf{e}_6\}_{\mathrm{span}}$
4	M_4	$\mathfrak{m}_4\triangleq\{\mathbf{e}_1,\mathbf{e}_2,\mathbf{e}_4,\mathbf{e}_5\}_{\mathrm{span}}$	$\{\mathbf{e}_3,\mathbf{e}_6\}_{\mathrm{span}}$	$\mathfrak{se}(3)$	$\exp\{\mathbf{e}_3,\mathbf{e}_6\}_{\mathrm{span}}$
5	M_5	$\mathfrak{m}_5\triangleq\{\mathbf{e}_1,\mathbf{e}_2,\mathbf{e}_3,\mathbf{e}_4,\mathbf{e}_5\}_{\mathrm{span}}$	$\{\mathbf{e}_1,\mathbf{e}_2,\mathbf{e}_3,\mathbf{e}_6\}_{\mathrm{span}}$	$\mathfrak{se}(3)$	$\exp\{\mathbf{e}_1,\mathbf{e}_2,\mathbf{e}_3,\mathbf{e}_6\}_{\mathrm{span}}$

Tab. B.1. This classification makes use of the canonical basis of $\mathfrak{se}(3)$ defined in Fig. A.1. A mD SS with one and two rotational DoFs is denoted by M_{mA} and M_{mB}, respectively. M_{4B} and M_{5B} are simply denoted by M_4 and M_5, since M_{4A} and M_{5A} do not exist. For reference, we also recall the screw systems of the Lie triple subsystems corresponding to the symmetric subspaces in Fig. B.1, and their symmetric twist pairs in Fig. B.2.

APPENDIX C
PROOF OF THEOREM 1

For clarity, we shall drop the leg index i in this proof. According to [13, Prop. 2(c)], since $\boldsymbol{\xi}_j^+\in\mathfrak{g}_\mathfrak{m}, j=1,...,k$, we may assume (by taking θ_j's to be small enough) that $e^{\theta_1\boldsymbol{\xi}_1^+}...e^{\theta_k\boldsymbol{\xi}_k^+}$ is contained in the coordinate neighborhood of $\mathbf{I}$ in $\mathrm{G_M}$ defined by $\widetilde{\exp}_\mathbf{I}:\mathfrak{m}\times\mathfrak{h}_\mathfrak{m}\to\mathrm{G_M}$. Therefore, there exists $\boldsymbol{\xi}\in\mathfrak{m}$ and $\boldsymbol{\eta}\in\mathfrak{h}_\mathfrak{m}$ such that

$$e^{\theta_1\boldsymbol{\xi}_1^+}...e^{\theta_k\boldsymbol{\xi}_k^+}=e^{\boldsymbol{\xi}}e^{\boldsymbol{\eta}} \tag{C.1}$$

To prove Eq. (21), we may simply proceed by induction.

For $k=1$, given $e^{\theta_1\boldsymbol{\xi}_1^+}=e^{\boldsymbol{\xi}}e^{\boldsymbol{\eta}}$ for $\boldsymbol{\xi}\in\mathfrak{m}$ and $\boldsymbol{\eta}\in\mathfrak{h}_\mathfrak{m}$, we apply the Campbell-Baker-Hausdorff-Dynkin (CBHD) formula [85]:

$$\begin{aligned}\theta_1\boldsymbol{\xi}_1^+&=\log(e^{\boldsymbol{\xi}}e^{\boldsymbol{\eta}})=\boldsymbol{\xi}+\boldsymbol{\eta}+\frac{1}{2}[\boldsymbol{\xi},\boldsymbol{\eta}]+\\&\frac{1}{12}([\boldsymbol{\xi},[\boldsymbol{\xi},\boldsymbol{\eta}]]+[\boldsymbol{\eta},[\boldsymbol{\eta},\boldsymbol{\xi}]])+\text{h.o.t.}\\&=\Sigma_0+\Sigma_1\end{aligned} \tag{C.2}$$

where Σ_0 and Σ_1 are summations of terms in the CBHD formula involving an even and an odd number of $\boldsymbol{\xi}$'s respectively (rearrangement is allowed since the CBHD formula is absolutely convergent for $\|\boldsymbol{\xi}\|<1,\|\boldsymbol{\eta}\|<1$ [86]). By the definition of LTS $\mathfrak{m}$ and $\mathfrak{h}_\mathfrak{m}$:

$$[\mathfrak{m},\mathfrak{m}]=\mathfrak{h}_\mathfrak{m},\quad [\mathfrak{h}_\mathfrak{m},\mathfrak{m}]\subset\mathfrak{m},\quad [\mathfrak{h}_\mathfrak{m},\mathfrak{h}_\mathfrak{m}]\subset\mathfrak{h}_\mathfrak{m} \tag{C.3}$$

one may easily show that $\Sigma_0\in\mathfrak{h}_\mathfrak{m}$ and $\Sigma_1\in\mathfrak{m}$. By the construction of SP $(\boldsymbol{\xi}_1^+,\boldsymbol{\xi}_1^-)$ given in Eq. (12),

$$\begin{cases}\boldsymbol{\xi}_1^+=\boldsymbol{\xi}_1+\boldsymbol{\eta}_1\\ \boldsymbol{\xi}_1^-=\boldsymbol{\xi}_1-\boldsymbol{\eta}_1\end{cases}\qquad \boldsymbol{\xi}_1\in\mathfrak{m},\boldsymbol{\eta}_1\in\mathfrak{h}_\mathfrak{m} \tag{C.4}$$

We see that $\Sigma_0=\theta_1\boldsymbol{\eta}_1$ and $\Sigma_1=\theta_1\boldsymbol{\xi}_1$. On the other hand, we have:

$$\log(e^{-\boldsymbol{\xi}}e^{\boldsymbol{\eta}})=\Sigma_0-\Sigma_1=-\theta_1(\boldsymbol{\xi}_1-\boldsymbol{\eta}_1)=-\theta_1\boldsymbol{\xi}_1^- \tag{C.5}$$

and therefore $e^{-\theta_1\boldsymbol{\xi}_1^-}=e^{-\boldsymbol{\xi}}e^{\boldsymbol{\eta}}$.

Next, assume the statement is true for $k=n-1$, that is, we have:

$$\begin{cases}e^{\theta_2\boldsymbol{\xi}_2^+}...e^{\theta_n\boldsymbol{\xi}_n^+}=e^{\boldsymbol{\xi}}e^{\boldsymbol{\eta}}\\ e^{-\theta_2\boldsymbol{\xi}_2^-}...e^{-\theta_n\boldsymbol{\xi}_n^-}=e^{-\boldsymbol{\xi}}e^{\boldsymbol{\eta}}\end{cases} \tag{C.6}$$

for some $\boldsymbol{\xi}\in\mathfrak{m}$ and $\boldsymbol{\eta}\in\mathfrak{h}_\mathfrak{m}$ (note that the case $k=n-1$ also implies $k<n-1$ by letting $\boldsymbol{\xi}_j^\pm=0, j=2,...,n-k$). Then we have for $k=n$:

$$\begin{cases}e^{\theta_1\boldsymbol{\xi}_1^+}...e^{\theta_n\boldsymbol{\xi}_n^+}=e^{\theta_1\boldsymbol{\xi}_1^+}e^{\boldsymbol{\xi}}e^{\boldsymbol{\eta}}\\ e^{-\theta_1\boldsymbol{\xi}_1^-}...e^{-\theta_n\boldsymbol{\xi}_n^-}=e^{-\theta_1\boldsymbol{\xi}_1^-}e^{-\boldsymbol{\xi}}e^{\boldsymbol{\eta}}\end{cases} \tag{C.7}$$

Observe that we have from $k=2$:

$$\begin{cases}e^{\theta_1\boldsymbol{\xi}_1^+}e^{\boldsymbol{\xi}}=e^{\boldsymbol{\xi}'}e^{\boldsymbol{\eta}'}\\ e^{-\theta_1\boldsymbol{\xi}_1^-}e^{-\boldsymbol{\xi}}=e^{-\boldsymbol{\xi}'}e^{\boldsymbol{\eta}'}\end{cases} \tag{C.8}$$

for some $\boldsymbol{\xi}'\in\mathfrak{m}$ and $\boldsymbol{\eta}'\in\mathfrak{h}_\mathfrak{m}$. Substitute Eq. (C.8) back into Eq. (C.7), and notice that $e^{\boldsymbol{\eta}'}e^{\boldsymbol{\eta}}=e^{\boldsymbol{\eta}''}$ for some $\boldsymbol{\eta}''\in\mathfrak{h}_\mathfrak{m}$ (since $\mathfrak{h}_\mathfrak{m}$ is a Lie subalgebra), and we have:

$$\begin{cases}e^{\theta_1\boldsymbol{\xi}_1^+}...e^{\theta_n\boldsymbol{\xi}_n^+}=e^{\boldsymbol{\xi}'}e^{\boldsymbol{\eta}''}\\ e^{-\theta_1\boldsymbol{\xi}_1^-}...e^{-\theta_n\boldsymbol{\xi}_n^-}=e^{-\boldsymbol{\xi}'}e^{\boldsymbol{\eta}''}\end{cases} \tag{C.9}$$

The mathematical induction is now complete. □

APPENDIX D
NON-EXISTENCE OF POE REPRESENTATION FOR SYMMETRIC SUBSPACES

***Proposition* 1.** Given a symmetric subspace $\exp\mathfrak{m}$ of $\mathrm{SE}(3)$ that is not a Lie subgroup (i.e., the Lie triple subsystem $\mathfrak{m}$ is not a Lie subalgebra of $\mathfrak{se}(3)$), $\exp\mathfrak{m}$ admits no POE representation.

Proof. Suppose that

$$\prod_{j=1}^{k}\exp\{\boldsymbol{\xi}_j\}_{\mathrm{span}}:=\{e^{\theta_1\boldsymbol{\xi}_1}...e^{\theta_k\boldsymbol{\xi}_k}\mid\theta_j\in(-\varepsilon,\varepsilon),\varepsilon>0\} \tag{D.1}$$

is a POE representation of $\exp\mathfrak{m}$. The fact that the identity tangent space of $\prod_{j=1}^k\exp\{\boldsymbol{\xi}_j\}_{\mathrm{span}}$ is given by $\{\boldsymbol{\xi}_1,...,\boldsymbol{\xi}_k\}_{\mathrm{span}}$ implies:

$$\{\boldsymbol{\xi}_1,...,\boldsymbol{\xi}_k\}_{\mathrm{span}}=\mathfrak{m} \tag{D.2}$$

Since $\mathfrak{m}$ is not a Lie subalgebra, we have at least two twists $\boldsymbol{\xi}_r,\boldsymbol{\xi}_s, 1\le r<s\le k$, such that $[\boldsymbol{\xi}_r,\boldsymbol{\xi}_s]\notin\mathfrak{m}$.

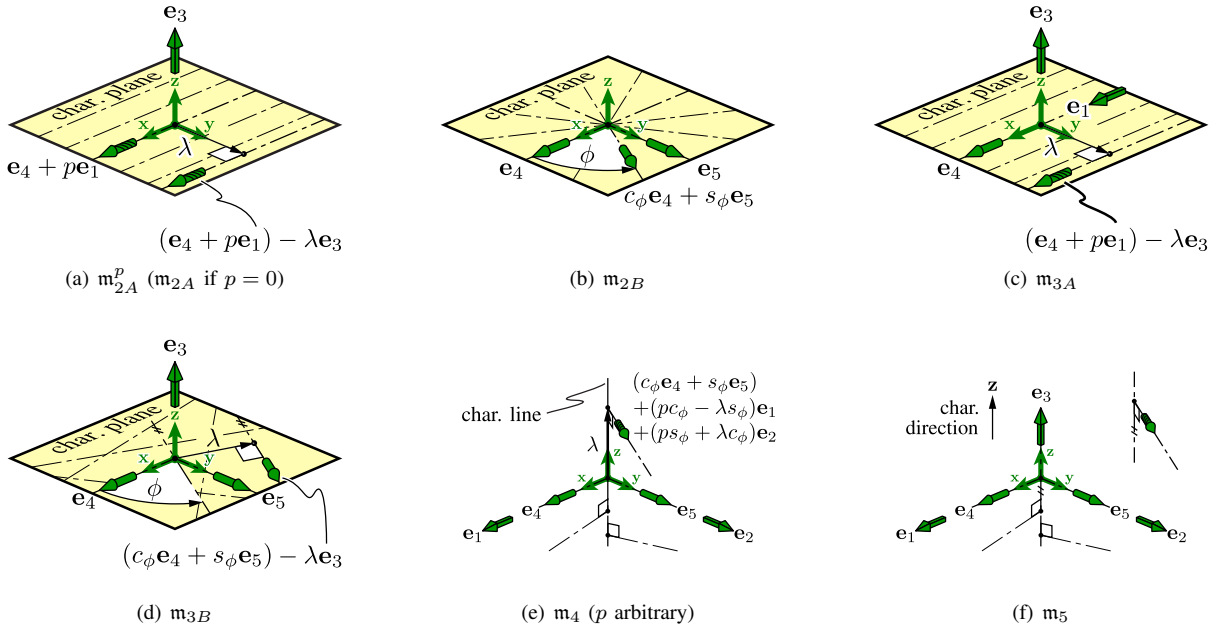

(a) $\mathfrak{m}_{2A}^p$ ($\mathfrak{m}_{2A}$ if $p = 0$) (b) $\mathfrak{m}_{2B}$ (c) $\mathfrak{m}_{3A}$

(d) $\mathfrak{m}_{3B}$ (e) $\mathfrak{m}_4$ (p arbitrary) (f) $\mathfrak{m}_5$

Fig. B.1. Screw systems of Lie triple subsystems. The basis screws along with a generic screw are shown for each $\mathfrak{m}$ (green arrows). The characteristic plane of $\mathfrak{m}_{2A}^p$ ($\mathfrak{m}_{2A}$), $\mathfrak{m}_{2B}$, $\mathfrak{m}_{3A}$, $\mathfrak{m}_{3B}$ is defined as the plane containing the axes of all finite-pitch screws. The characteristic line of $\mathfrak{m}_4$ is defined as the line that intersects all finite-pitch screws at right angle. The characteristic direction of $\mathfrak{m}_5$ is defined as the direction perpendicular to all finite-pitch screws. $c_{(\cdot)}$ and $s_{(\cdot)}$ denote $\cos(\cdot)$ and $\sin(\cdot)$ respectively.

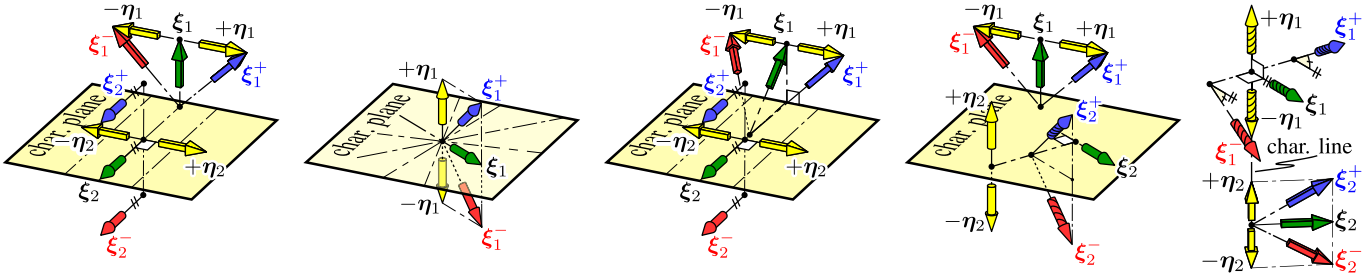

(a) $\mathfrak{m}_{2A}^{(p)}$ (b) $\mathfrak{m}_{2B}$ (c) $\mathfrak{m}_{3A}$ (d) $\mathfrak{m}_{3B}$ (e) $\mathfrak{m}_4$

Fig. B.2. Symmetric twist pairs of LTSs. Since $\mathfrak{m}_5$ contains all other LTSs, all the above SPs are also SPs of $\mathfrak{m}_5$.

Now a contradiction is constructed as follows. First, note that the 2D submanifold $\exp\{\boldsymbol{\xi}_r\}_{\text{span}} \cdot \exp\{\boldsymbol{\xi}_s\}_{\text{span}}$ of $\prod_{j=1}^k \exp\{\boldsymbol{\xi}_j\}_{\text{span}}$ is locally contained in $\exp\mathfrak{m}$ (this is true even if $\boldsymbol{\xi}_r$ and $\boldsymbol{\xi}_s$ are not adjacent). We apply the CBHD formula [85] to construct a curve $\mathfrak{c}(t)$ in $\mathfrak{m}$:

$$\begin{aligned}\mathfrak{c}(t) :=& \log(e^{t\boldsymbol{\xi}_r} e^{t\boldsymbol{\xi}_s}) \\ =& t\boldsymbol{\xi}_r + t\boldsymbol{\xi}_s + \frac{t^2}{2}[\boldsymbol{\xi}_r, \boldsymbol{\xi}_s] + O(t^3), \quad t \in (-\varepsilon, \varepsilon)\end{aligned} \tag{D.3}$$

Since $\mathfrak{m}$ is a vector space, we have:

$$\frac{d\mathfrak{c}(t)}{dt} = \lim_{\delta t \to 0} \frac{\mathfrak{c}(t+\delta t) - \mathfrak{c}(t)}{\delta t} \in \mathfrak{m} \tag{D.4}$$

and also

$$\begin{aligned}\left.\frac{d^2\mathfrak{c}(t)}{dt^2}\right|_{t=0} =& \lim_{\delta t \to 0} \left(\left.\frac{d\mathfrak{c}(u)}{du}\right|_{u=\delta t} - \left.\frac{d\mathfrak{c}(u)}{du}\right|_{u=0} \right) \\ =& [\boldsymbol{\xi}_r, \boldsymbol{\xi}_s] \in \mathfrak{m}\end{aligned} \tag{D.5}$$

This completes the proof. □

References

[1] J. Hervé, "The Lie group of rigid body displacements, a fundamental tool for mechanism design," *Mechanism and Machine theory*, vol. 34, no. 5, pp. 719–730, 1999.

[2] J. M. Selig and J. Rooney, "Reuleaux pairs and surfaces that cannot be gripped," *The International Journal of Robotics Research*, vol. 8, no. 5, pp. 79–87, 1989.

[3] J.-Y. Wen and K. Kreutz-Delgado, "The attitude control problem," *Automatic Control, IEEE Transactions on*, vol. 36, no. 10, pp. 1148–1162, 1991.

[4] A. W. Long, K. C. Wolfe, M. Mashner, and G. S. Chirikjian, "The banana distribution is Gaussian: A localization study with exponential coordinates." in *Robotics: science and systems*, 2012.

[5] F. Pierrot, C. Reynaud, and A. Fournier, "DELTA: a simple and efficient parallel robot," *Robotica*, vol. 8, no. 2, pp. 105–109, 1990.

[6] F. Pierrot, V. Nabat, O. Company, S. Krut, and P. Poignet, "Optimal design of a 4-dof parallel manipulator: From academia to industry," *IEEE Transactions on Robotics*, vol. 25, no. 2, pp. 213–224, 2009.

[7] R. J. Popplestone, Y. Liu, and R. Weiss, "A group theoretic approach to assembly planning," *AI magazine*, vol. 11, no. 1, p. 82, 1990.

[8] Z. Li, J. Gou, and Y. Chu, "Geometric algorithms for workpiece localization," *IEEE Transactions on Robotics and Automation*, vol. 14, no. 6, pp. 864–878, 1998.

[9] B. Siciliano, L. Sciavicco, L. Villani, and G. Oriolo, *Robotics: modelling, planning and control*. Springer Science & Business Media, 2010.

[10] I. A. Bonev and J. Ryu, "A new approach to orientation workspace analysis of 6-DOF parallel manipulators," *Mechanism and machine theory*, vol. 36, no. 1, pp. 15–28, 2001.

[11] X. Kong, "Reconfiguration analysis of a 3-dof parallel mechanism using euler parameter quaternions and algebraic geometry method," *Mechanism and Machine Theory*, vol. 74, pp. 188–201, 2014.

[12] Y. Wu and M. Carricato, "Identification and geometric characterization of Lie triple screw systems and their exponential images," *Mechanism and Machine Theory*, vol. 107, pp. 305–323, 2017.

[13] Y. Wu, H. Löwe, M. Carricato, and Z. Li, "Inversion symmetry of the Euclidean group: Theory and application to robot kinematics," *IEEE Transactions on Robotics*, vol. 32, no. 2, pp. 312–326, 2016.

[14] O. Loos, *Symmetric spaces*. WA Benjamin, 1969, vol. 1.

[15] M. Berger, *Geometry I*. Springer Science & Business Media, 2009.

[16] H. Z. Munthe-Kaas, G. R. W. Quispel, and A. Zanna, "Symmetric spaces and Lie triple systems in numerical analysis of differential equations," *BIT Numerical Mathematics*, vol. 54, no. 1, pp. 257–282, 2014.

[17] Y. Wu, A. Müller, and M. Carricato, "The 2D orientation interpolation problem: a symmetric space approach," in *Advances in Robot Kinematics 2016*. Springer, 2018, pp. 293–302.

[18] S. Kobayashi and K. Nomizu, *Foundations of differential geometry*. Wiley New York, 1969, vol. 2.

[19] D. Tweed and T. Vilis, "Geometric relations of eye position and velocity vectors during saccades," *Vision research*, vol. 30, no. 1, pp. 111–127, 1990.

[20] A. D. Polpitiya, W. P. Dayawansa, C. F. Martin, and B. K. Ghosh, "Geometry and control of human eye movements," *Automatic Control, IEEE Transactions on*, vol. 52, no. 2, pp. 170–180, 2007.

[21] J. Selig and M. Husty, "Half-turns and line symmetric motions," *Mechanism and Machine Theory*, vol. 46, no. 2, pp. 156–167, 2011.

[22] G. S. Chirikjian and J. W. Burdick, "Kinematically optimal hyper-redundant manipulator configurations," *IEEE transactions on Robotics and Automation*, vol. 11, no. 6, pp. 794–806, 1995.

[23] A. Wingert, M. D. Lichter, and S. Dubowsky, "On the kinematics of parallel mechanisms with bi-stable polymer actuators," in *Advances in Robot Kinematics*. Springer, 2002, pp. 303–310.

[24] R. Behrens, M. Poggendorf, E. Schulenburg, and N. Elkmann, "An elephant's trunk-inspired robotic arm-trajectory determination and control," in *Robotics; Proceedings of ROBOTIK 2012; 7th German Conference on*. VDE, 2012, pp. 1–5.

[25] F. Renda, M. Cianchetti, H. Abidi, J. Dias, and L. Seneviratne, "Screw-based modeling of soft manipulators with tendon and fluidic actuation," *Journal of Mechanisms and Robotics*, vol. 9, no. 4, p. 041012, 2017.

[26] C.-H. Kuo and J. S. Dai, "Robotics for minimally invasive surgery: a historical review from the perspective of kinematics," in *International symposium on history of machines and mechanisms*. Springer, 2009, pp. 337–354.

[27] A. M. Dollar and H. Herr, "Lower extremity exoskeletons and active orthoses: challenges and state-of-the-art," *IEEE Transactions on robotics*, vol. 24, no. 1, pp. 144–158, 2008.

[28] A. H. Stienen, E. E. Hekman, F. C. Van Der Helm, and H. Van Der Kooij, "Self-aligning exoskeleton axes through decoupling of joint rotations and translations," *IEEE Transactions on Robotics*, vol. 25, no. 3, pp. 628–633, 2009.

[29] N. Jarrassé and G. Morel, "Connecting a human limb to an exoskeleton," *IEEE Transactions on Robotics*, vol. 28, no. 3, pp. 697–709, 2012.

[30] M. Cempini, S. M. M. De Rossi, T. Lenzi, N. Vitiello, and M. C. Carrozza, "Self-alignment mechanisms for assistive wearable robots: a kinetostatic compatibility method," *IEEE Transactions on Robotics*, vol. 29, no. 1, pp. 236–250, 2013.

[31] N. Vitiello, T. Lenzi, S. Roccella, S. M. M. De Rossi, E. Cattin, F. Giovacchini, F. Vecchi, and M. C. Carrozza, "Neuroexos: A powered elbow exoskeleton for physical rehabilitation," *IEEE Transactions on Robotics*, vol. 29, no. 1, pp. 220–235, 2013.

[32] Q. Li, Z. Huang, and J. M. Hervé, "Type synthesis of 3R2T 5-DOF parallel mechanisms using the Lie group of displacements," *IEEE transactions on robotics and automation*, vol. 20, no. 2, pp. 173–180, 2004.

[33] J. Meng, G. Liu, Z. Li *et al.*, "A geometric theory for analysis and synthesis of sub-6 DoF parallel manipulators," *IEEE Transactions on Robotics*, vol. 23, no. 4, pp. 625–649, 2007.

[34] X. Kong and C. M. Gosselin, *Type synthesis of parallel mechanisms*. Springer, 2007.

[35] M. Carricato and D. Zlatanov, "Persistent screw systems," *Mechanism and Machine Theory*, vol. 73, pp. 296–313, 2014.

[36] Z. Huang and Q. Li, "Type synthesis of symmetrical lower-mobility parallel mechanisms using the constraint-synthesis method," *The International Journal of Robotics Research*, vol. 22, no. 1, pp. 59–79, 2003.

[37] M. Carricato, "Fully isotropic four-degrees-of-freedom parallel mechanisms for Schönflies motion," *The International Journal of Robotics Research*, vol. 24, no. 5, pp. 397–414, 2005.

[38] C.-C. Lee and J. M. Hervé, "Translational parallel manipulators with doubly planar limbs," *Mechanism and Machine Theory*, vol. 41, no. 4, pp. 433–455, 2006.

[39] K. Hunt, "Constant-velocity shaft couplings: a general theory," *Journal of Engineering for Industry*, vol. 95, no. 2, pp. 455–464, 1973.

[40] M. Carricato, "Decoupled and homokinetic transmission of rotational motion via constant-velocity joints in closed-chain orientational manipulators," *Journal of Mechanisms and Robotics*, vol. 1, no. 4, pp. 1–14, 2009.

[41] C. Li, Y. Wu, H. Löwe, and Z. Li, "POE-based robot kinematic calibration using axis configuration space and the adjoint error model," *IEEE Transactions on Robotics*, vol. 32, no. 5, pp. 1264–1279, 2016.

[42] W. Hong, A. Y. Yang, K. Huang, and Y. Ma, "On symmetry and multiple-view geometry: Structure, pose, and calibration from a single image," *International Journal of Computer Vision*, vol. 60, no. 3, pp. 241–265, 2004.

[43] R. Tron and K. Daniilidis, "The space of essential matrices as a riemannian quotient manifold," *SIAM Journal on Imaging Sciences*, 2017.

[44] J. Hervé and F. Sparacino, "Structural synthesis of parallel robots generating spatial translation," in *Proceedings of the 5th IEEE international conference on advanced robotics*, 1991, pp. 808–813.

[45] Y. Wu, H. Wang, and Z. Li, "Quotient kinematics machines: Concept, analysis, and synthesis," *Journal of mechanisms and robotics*, vol. 3, no. 4, p. 041004, 2011.

[46] M. Carricato and V. Parenti-Castelli, "Singularity-free fully-isotropic translational parallel mechanisms," *The International Journal of Robotics Research*, vol. 21, no. 2, pp. 161–174, 2002.

[47] ——, "A novel fully decoupled two-degrees-of-freedom parallel wrist," *The International Journal of Robotics Research*, vol. 23, no. 6, pp. 661–667, 2004.

[48] Z. Huang and Q. Li, "General methodology for type synthesis of symmetrical lower-mobility parallel manipulators and several novel manipulators," *The International Journal of Robotics Research*, vol. 21, no. 2, pp. 131–145, 2002.

[49] Y. Fang and L.-W. Tsai, "Structure synthesis of a class of 4-DoF and 5-DoF parallel manipulators with identical limb structures," *The international journal of Robotics Research*, vol. 21, no. 9, pp. 799–810, 2002.

[50] ——, "Structure synthesis of a class of 3-DOF rotational parallel manipulators," *IEEE transactions on robotics and automation*, vol. 20, no. 1, pp. 117–121, 2004.

[51] X. Kong and G. C. M, "Type synthesis of 3-DOF translational parallel manipulators based on screw theory," *Journal of Mechanical Design*, vol. 126, no. 1, pp. 83–92, 2004.

[52] X. Kong and C. M. Gosselin, "Type synthesis of 3T1R 4-DOF parallel manipulators based on screw theory," *IEEE transactions on robotics and automation*, vol. 20, no. 2, pp. 181–190, 2004.

[53] ——, "Type synthesis of three-degree-of-freedom spherical parallel manipulators," *The International Journal of Robotics Research*, vol. 23, no. 3, pp. 237–245, 2004.

[54] I. Bonev, D. Zlatanov, and C. Gosselin, "Advantages of the modified Euler angles in the design and control of PKMs," in *2002 Parallel Kinematic Machines International Conference*, 2002, pp. 171–188.

[55] J. selig, "A class of explicitly solvable vehicle motion problems," *IEEE Transactions on Robotics*, vol. 31, no. 3, pp. 766–777, 2015.

[56] E. Gawlik and M. Leok, "Interpolation on symmetric spaces via the generalized polar decomposition," *arXiv preprint arXiv:1605.06666*, 2016.

[57] K. H. Hunt, *Kinematic geometry of mechanisms*. Oxford University Press, 1978.

[58] M. Zoppi, D. Zlatanov, and R. Molfino, "On the velocity analysis of interconnected chains mechanisms," *Mechanism and machine theory*, vol. 41, no. 11, pp. 1346–1358, 2006.

[59] H. Löwe, Y. Wu, and M. Carricato, "Symmetric subspaces of $\mathrm{SE}(3)$," *Advances in Geometry*, 2016.

[60] Y. Wu and M. Carricato, "Design of a novel 3-dof serial-parallel robotic wrist: A symmetric space approach," in *Robotics Research*. Springer, 2018, pp. 389–404.

[61] X. Kong, "Forward displacement analysis of a 2-dof RR-RRR-RRR spherical parallel manipulator," in *Mechatronics and Embedded Systems and Applications (MESA), 2010 IEEE/ASME International Conference on*. IEEE, 2010, pp. 446–451.

[62] C. M. Gosselin and J.-F. Hamel, "The agile eye: a high-performance three-degree-of-freedom camera-orienting device," in *Robotics and Automation, 1994. Proceedings., 1994 IEEE International Conference on*. IEEE, 1994, pp. 781–786.

[63] M. E. Rosheim and G. F. Sauter, "New high-angulation omni-directional sensor mount," in *Proceedings of SPIE - The International Society for Optical Engineering*, vol. 4821, 2002, pp. 163–174.

[64] X.-S. Gao, D. Lei, Q. Liao, and G.-F. Zhang, "Generalized Stewart–Gough platforms and their direct kinematics," *IEEE Transactions on Robotics*, vol. 21, no. 2, pp. 141–151, 2005.

[65] J. E. McInroy and F. Jafari, "Finding symmetric orthogonal Gough–Stewart platforms," *IEEE transactions on robotics*, vol. 22, no. 5, pp. 880–889, 2006.

[66] J. Borras, F. Thomas, and C. Torras, "New geometric approaches to the analysis and design of Stewart-Gough platforms," *IEEE/ASME Transactions on Mechatronics*, vol. 19, no. 2, pp. 445–455, 2014.

[67] C. Gosselin and L.-T. Schreiber, "Kinematically redundant spatial parallel mechanisms for singularity avoidance and large orientational workspace," *IEEE Transactions on Robotics*, vol. 32, no. 2, pp. 286–300, 2016.

[68] H. Löwe and Y. Wu, "Exponential pairs of subspaces of $\mathfrak{se}(3)$," 2017, in preparation.

[69] L. J. Stocco, S. E. Salcudean, and F. Sassani, "Optimal kinematic design of a haptic pen," *Mechatronics, IEEE/ASME Transactions on*, vol. 6, no. 3, pp. 210–220, 2001.

[70] R. P. Paul and C. N. Stevenson, "Kinematics of robot wrists," *The International journal of robotics research*, vol. 2, no. 1, pp. 31–38, 1983.

[71] Y. Wu and M. Carricato, "Optimal design of N-$\mathcal{UU}$ parallel mechanisms," in *Computational Kinematics*. Springer, 2018, pp. 394–402.

[72] J. Kim, F. C. Park, S. J. Ryu, J. Kim, J. C. Hwang, C. Park, and C. C. Iurascu, "Design and analysis of a redundantly actuated parallel mechanism for rapid machining," *IEEE Transactions on robotics and automation*, vol. 17, no. 4, pp. 423–434, 2001.

[73] Y. Chen and F. Dong, "Robot machining: recent development and future research issues," *The International Journal of Advanced Manufacturing Technology*, pp. 1–9, 2013.

[74] O. Bottema and B. Roth, *Theoretical kinematics*. North Holland Publishing Co., 1979.

[75] M. Zefran, V. Kumar, and C. B. Croke, "On the generation of smooth three-dimensional rigid body motions," *IEEE Transactions on Robotics and Automation*, vol. 14, no. 4, pp. 576–589, 1998.

[76] N. Kumar, "Design and development of devices for robotized needle insertion procedures," Ph.D. dissertation, Université de Strasbourg, 2014.

[77] C.-H. Kuo and J. S. Dai, "Kinematics of a fully-decoupled remote center-of-motion parallel manipulator for minimally invasive surgery," *Journal of Medical Devices*, vol. 6, no. 2, p. 021008, 2012.

[78] Q. Li, J. M. Hervé, and P. Huang, "Type synthesis of a special family of remote center-of-motion parallel manipulators with fixed linear actuators for minimally invasive surgery," *Journal of Mechanisms and Robotics*, vol. 9, no. 3, p. 031012, 2017.

[79] N. Kumar, O. Piccin, and B. Bayle, "A task-based type synthesis of novel 2T2R parallel mechanisms," *Mechanism and Machine Theory*, vol. 77, pp. 59–72, 2014.

[80] D. A. Neumann, *Kinesiology of the musculoskeletal system: foundations for rehabilitation*. Elsevier Health Sciences, 2013.

[81] V. Parenti-Castelli, A. Leardini, R. Di Gregorio, and J. J. O'connor, "On the modeling of passive motion of the human knee joint by means of equivalent planar and spatial parallel mechanisms," *Autonomous Robots*, vol. 16, no. 2, pp. 219–232, 2004.

[82] R. Di Gregorio, V. Parenti-Castelli, J. J. OConnor, and A. Leardini, "Mathematical models of passive motion at the human ankle joint by equivalent spatial parallel mechanisms," *Medical & biological engineering & computing*, vol. 45, no. 3, pp. 305–313, 2007.

[83] R. M. Murray, Z. Li, S. S. Sastry, and S. S. Sastry, *A mathematical introduction to robotic manipulation*. CRC press, 1994.

[84] J. K. Davidson and K. H. Hunt, *Robots and screw theory: applications of kinematics and statics to robotics*. Oxford University Press, 2004.

[85] A. Bonfiglioli and R. Fulci, *Topics in noncommutative algebra: the theorem of Campbell, Baker, Hausdorff and Dynkin*. Springer Science & Business Media, 2011, vol. 2034.

[86] S. Blanes and F. Casas, "On the convergence and optimization of the Baker–Campbell–Hausdorff formula," *Linear algebra and its applications*, vol. 378, pp. 135–158, 2004.

Yuanqing Wu (M'17–) received his B.Sc. degree in mechanical engineering in 2001 and Ph.D. degree in mechatronics engineering in 2009, both from Shanghai Jiaotong University, China.

He was first a research assistant and later a research associate at the Electronic and Computer Engineering Department, Hong Kong University of Science and Technology, China. He is currently a contract researcher with the Department of Industrial Engineering, University of Bologna. His research interests includes kinematic geometry, mechanism theory, parallel robots, geometric control and geometric algebra computing.

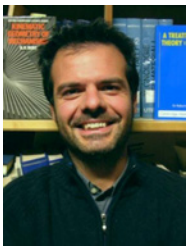

Marco Carricato (M'10–) received the M.Sc. degree (with honors) in mechanical engineering in 1998 and the Ph.D. degree in mechanics of machines in 2002. He has been with the University of Bologna since 2004. He is currently an associate professor.

He was visiting researcher at the University of Florida (USA), at Laval University (Canada), at the University of Guanajuato (Mexico), at INRIA–Sophia Antipolis (France), at the Ecole Centrale of Nantes (France), and at the Hong Kong University of Science and Technology. He is an associate editor of the journal Mechanism and Machine Theory. He was awarded the AIMETA Junior Prize 2011 by the Italian Association of Theoretical and Applied Mechanics for outstanding results in the field of mechanics of machines. His research interests include robotic systems, servo-actuated automatic machinery and the theory of mechanisms, with a particular emphasis on parallel manipulators, efficiency and optimization of servomechanisms, the theory of screws, and the theory of homokinetic couplings.